Highly Selective Determination of Copper Corrosion Products by Voltammetric Reduction

中山, 茂吉

(Degree)
博士（理学）

(Date of Degree)
2013-03-06

(Date of Publication)
2013-05-02

(Resource Type)
doctoral thesis

(Report Number)
乙3209

(URL)
https://hdl.handle.net/20.500.14094/D2003209

神戸大学博士論文

Highly Selective Determination of Copper Corrosion Products by Voltammetric Reduction

ボルタンメトリー還元法による銅腐食生成物の高選択的定量法

平成 25 年 1 月

中山　茂吉

Table of Contents

Chapter 5. Growth Mechanism of Copper Oxides

Chapter 6. Application to Tin

Summary

Chapter 1. Introduction

1.1. Overview

Copper is the metal that has been used longest by mankind since thousands of years ago. Besides the relatively high corrosion resistance, copper has characteristics of high electrical and thermal conductivities. Therefore, copper and its alloys have been widely used to fabricate industrial products, coins, and artifacts. When copper is exposed to air-containing moisture and pollutants, however, various corrosion products are formed on copper surfaces. It is generally known that cuprous oxide (Cu_2O) forms at an early stage of the corrosion process. Upon further oxidation, a new top layer of cupric oxide (CuO) grows preferentially over the Cu_2O layer.[2,3] Eventually, corrosion products on copper change to a stable patina.[1,4] In addition, copper sulfides, mainly cupric sulfide (Cu_2S), are formed on copper surfaces in air containing H_2S[2,5-7] or in a solution containing S^{2-} ions.[8]

Copper corrosion products often have a bad influence on industrial products. Tarnishing by oxidation frequently reduces the commercial value of copper products. Problems such as defects of wire bonding,[9] stress corrosion cracking,[10] and contact resistance of connectors[11] have also been reported. Since the corrosion products formed on copper have different properties, their qualitative and quantitative analyses are important for clarification of the corrosion mechanism and for corrosion protection. For selective determination of copper corrosion products, surface analytical techniques such as X-ray photoelectron spectroscopy (XPS),[3, 12-14] X-ray diffraction (XRD),[6] and infrared reflection absorption spectroscopy (IRAS)[15] have been extensively employed. These spectroscopic techniques are very useful for qualitative analysis, but are not necessarily adequate for quantitative analysis.

Electrochemical techniques provide more reliable information on the “quantities” of copper corrosion products. Chronopotentiometry (CP) has been most frequently applied for quantitative analysis of copper oxides (Cu_2O and CuO) or cuprous sulfide (Cu_2S). However, this conventional

method has serious problems, including (1) an obscurity about the reduction order of copper oxides and (2) a worse separation between the reduction potentials of Cu_2O and CuO. The first report[16] published in 1937 for the use of CP claimed that the reduction of Cu_2O occurred firstly, followed by the reduction of CuO, however, no convincing evidence was presented. In recent years, some researchers claimed that the reduction order was "CuO → Cu_2O".[17-20] In Fig. 1.1, two conflicting views on the reduction order of copper oxides are schematically presented. Obviously, the analytical values for Cu_2O and CuO should depend on the view selected by a researcher. Coexistence of such two conflicting views has confused the researchers in the field of copper corrosion.

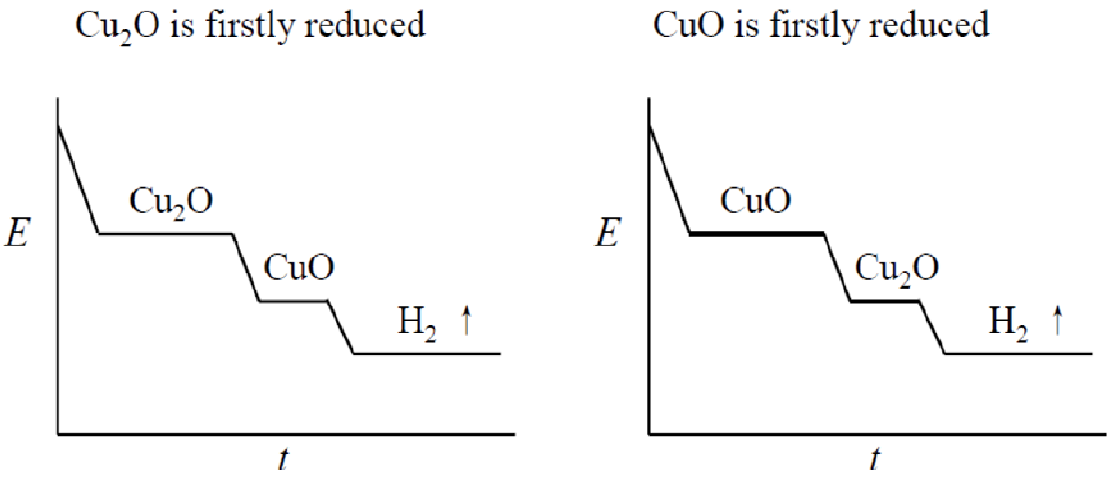

Figure 1.1 Two conflicting views on the reduction order of Cu_2O and CuO in CP measurements.

Linear sweep voltammetry (LSV) has also been frequently applied for the characterization of copper oxide films.[14,17,18] In this method as well, however, the current signals obtained for the reduction of Cu_2O and CuO are generally unclear and have insufficient separation.

In the previous electrochemical methods (*i.e.*, CP and LSV), a neutral or weak alkaline electrolyte (*e.g.*, 0.1 M (= mol dm^{-3}) KCl, 0.1 M Na_2CO_3 and 0.1 M $Na_2B_4O_7$, etc.) has been employed for the supporting electrolyte. These electrolytes seem to have been selected by taking

into consideration the stability of Cu_2O.[21,22]

1.2. Objective of this study

On the basis of the above-mentioned background, my coworkers and I carried out this study to develop a more reliable method for quantitative determination of copper corrosion products. The method selected is voltammetry, which provides, under appropriate measurement conditions, peak-like signals that are easy to analyze.

In Chapter 2, the outline of the developed method is described. First of all, I focused on the optimization of supporting electrolyte for achieving enough separation between the reduction peaks of Cu_2O and CuO. In order to study comprehensively the performance of the developed method, I prepared three standard samples (*i.e.*, Cu_2O/Cu[23], CuO/Cu[23] and $CuO/Cu_2O/Cu$[24]), which are schematically shown in Fig. 1.2. The thickness of copper oxide films in each sample was standardized to around 1 μm. To our knowledge, there have been only a few studies,[19,20] in which the reduction mechanism of copper oxides was investigated by using standard samples. However, the previous standard samples were composed of a rather thin and not fully identified oxide layer.

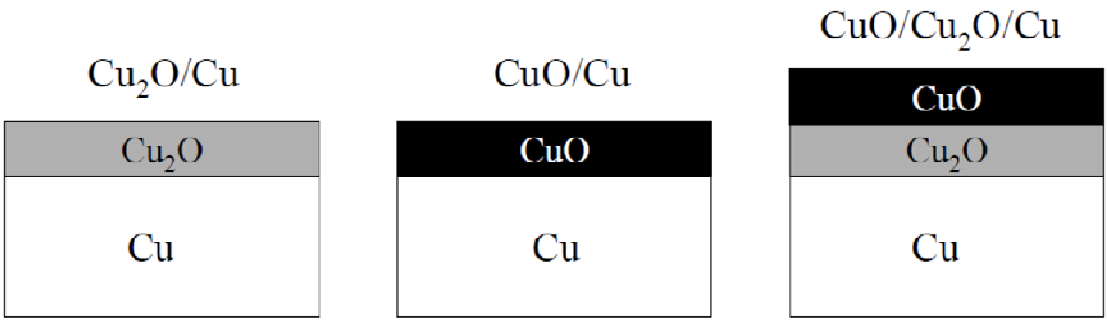

Figure 1.2 Schematic representation of the cross-sections of three standard samples.

By a detailed investigation, it was clarified that a strongly alkaline electrolyte (SAE)

composed of 6 M KOH + 1 M LiOH was very suitable for highly selective determination of copper oxides.[25] Two principal factors related to the advantages of SAE: *i.e.*, (1) Li^+ ions and (2) high alkalinity, were studied in some detail.[26] Impedance spectroscopy was employed to clarify the reduction mechanism, and the results are also shown in Chapter 2.

In Chapter 3, I focused on the reduction order of copper oxides (*i.e.*, Cu_2O and CuO). In the previous electrochemical measurements, a neutral electrolyte, 0.1 M KCl, was most frequently used as the supporting electrolyte for the detection of copper oxides and Cu_2S. In our recent study,[24] in order to clarify the reduction order of copper oxides, we prepared three different samples of Cu-duplex oxide films, and then compared the reduction behaviors of the oxides in 0.1 M KCl and SAE. It was then clearly shown that for the use of 0.1 M KCl, no clear separation could be achieved between the reduction potentials of Cu_2O and CuO.

So far, mainly the two oxides (*i.e.*, Cu_2O and CuO) have been analyzed by conventional electrochemical methods. In Chapter 4, further applications of the developed method to corrosion products other than oxides, which include sulfides, hydroxide, and "patina", are described. "Patina" is the general term for "rusts of copper" produced by long-term exposure to air,[1,4] and it refers to basic copper minerals which includes basic copper chlorides, sulfides, carbonates, and others. In this study, we obtained the results suggesting a possibility for the analysis of patinas using SAE.

In Chapter 5, the mechanism of atmospheric corrosion of copper, as studied by the developed method, is described. The use of SAE enabled us to propose a detailed growth mechanism of copper oxides. It was found that the surface layer of $Cu(OH)_2$ plays an important role in the initial stage of the atmospheric corrosion.

In the final chapter, a successful extension of the developed technique to another metal, *i.e.*, tin, is described.

References

1. T. E. Graedel, K. Nassau and J. P. Franey, *Corros. Sci.*, **27**, 639 (1987).
2. J. Kruger, *J. Electrochem. Soc.*, **106**, 847 (1959).
3. Y. Y. Su and R. M. Shemenski, *Surf. Interface Anal.*, **40**, 1183 (2008).
4. T. E. Graedel, *Corros. Sci.*, **27**, 721 (1987).
5. W. E. Campbell and U. B. Thomas, *Trans. Electrochem. Soc.,* **76**, 303 (1939).
6. S. P. Sharma, *J. Electrochem. Soc.*, **127**, 21 (1980).
7. M. Watanabe, M. Tomita and T. Ichino, *J. Electrochem. Soc.*, **149**, B97 (2002).
8. J. M. Smith, J. C. Wren, M. Odziemkowski and D. W. Shoesmith, *J. Electrochem. Soc.*, **154**, C431 (2007).
9. M. Soeda and R. Ozaki, *Journal of the JRICu*, **29**, 57 (1990).
10. A. J. McEvily, Jr. and A. P. Bond, *J. Electrochem. Soc.*, **112**, 131 (1965).
11. W. H. Abbott, *Mater. Performance*, **24**, 46 (1985).
12. S. K. Chawla, N. Sankarraman and J.H. Payer, *J. Electron. Spectrosc. Relat. Phenom.*, **61**, 1 (1992).
13. F. M. Al-Kharafi and B. G. Ateya, *J. Electrochem. Soc.*, **149**, B206 (2002).
14. T. T. M. Tran, C. Fiaud, E. M. M. Sutter and A. Villanova, *Corros. Sci.*, **45**, 2787 (2003).
15. J. Y. Malvault, J. Lopitaux, D. Delahaye and M. Lenglet, *J. Appl. Electrochem.*, **25**, 841 (1995).
16. H. A. Miley, *J. Am. Chem. Soc.*, **59**, 2626 (1937).
17. R. L. Deutscher and R. Woods, *J. Appl. Electrochem.*, **16**, 413 (1986).
18. M. Lenglet, K. Kartouni and D. Delahaye, *J. Appl. Electrochem.*, **21**, 697 (1991).
19. Y. Y. Su and M. Marek , *J. Electrochem. Soc.*, **141**, 940 (1994).
20. M. Seo, Y. Ishikawa, M. Kodaira, A. Sugimoto, S. Nakayama, M. Watanabe, S. Furuya, R. Minamitani, Y. Miyata, A. Nishikata and T. Notoya, *Corros. Sci.*, **47**, 2079 (2005).

21. R. R. H. Lanbert and D. J. Trevoy, *J. Electrochem. Soc.*, **105**, 18 (1958).

22. M. Pourbaix, " Atlas of Electrochemical Equilibria inAqueous Solutions, 2nd English ed.", p.387, NACE, Houston, TX (1974).

23. S. Nakayama, M. Shibata, T. Notoya and T. Osakai, *Bunseki Kagaku*, **51**, 1145 (2002).

24. S. Nakayama, T. Kaji, T. Notoya and T. Osakai, *J. Electrochem. Soc.*, **154**, C1 (2007).

25. S. Nakayama, A. Kimura, M. Shibata, S. Kuwabata and T. Osakai, *J. Electrochem. Soc.*, **148**, B467 (2001).

26. S. Nakayama, T. Kaji, T. Notoya and T. Osakai, *Electrochim. Acta*, **53**, 3493 (2008).

Chapter 2. Outline of the Developed Method

2.1. Introduction

A CP method for the determination of Cu_2O and CuO was firstly reported by Miley in 1937.[1] Since then, CP or LSV using a neutral or weak alkaline electrolyte such as 0.1 M KCl,[2-7] 0.1 M Na_2CO_3,[8-9] and 0.1 M $Na_2B_4O_7$[10-12] has been employed. These electrolytes seem to have been selected for the stability of Cu_2O.[13] However, only a low separation of the peaks of two oxides was obtained in such neutral or weak alkaline electrolytes, especially for the samples composed of relatively thick oxides films.

In this study, however, I fortuitously discovered that a strongly alkaline electrolyte (6 M KOH + 1 M LiOH; denoted as SAE) can provide an excellent separation between the reduction peaks of Cu_2O and CuO. In this chapter, I focused on the optimization of supporting electrolyte for achieving enough separation between the reduction peaks in LSV. The results will be presented while showing the outline of the developed method with SAE.

2.2. Experimental

2.2.1. Samples

Three standard samples shown in Fig. 1.1 were prepared as follows:

Dumet wire (JIS H 4541, Sumitomo Electric Ind., 0.71-mm ϕ) for glass-to-metal seal applications was used as a Cu_2O/Cu sample.[14] This wire is composed of an inner layer of Fe–Ni alloy and an outer layer of Cu plating (*ca*. 100-μm thick), the surface being thermally oxidized to form a Cu_2O layer (*ca*. 1.2-μm thick).

A CuO/Cu sample[14] was prepared in the following manner. An oxygen-free copper sheet (0.2-mm thick; JIS C15150, Mitsubishi Shindo Co. Ltd.) was cut to the size of 5 mm × 50 mm and then treated with commercially available solutions[15] (AD-331, MB-438A, MB-438B; Meltex Inc.) to form a 0.7-μm thick film of CuO on the copper surface.

A $CuO/Cu_2O/Cu$ sample[16] was prepared by immersion of a Cu_2O/Cu sample in 0.5 M NaOH at 30 °C for 32 h, resulting in partial oxidization of the surface of Cu_2O to CuO.

2.2.2. Electrochemical measurements

As shown in Fig. 2.1, a conventional three electrode electrolytic cell was employed for electrochemical measurements. Three standard samples were served as the working electrode (WE). An Ag/AgCl in 3 M NaCl electrode was used as the reference electrode (RE), to which all potentials are referred in this doctoral thesis. A platinum wire was used as the counter electrode (CE). The electrolyte solutions used were 0.1 M KCl, 1 M KOH, 1 M NaOH, 1 M LiOH, and 6 M KOH + 1 M LiOH, all of which were not deaerated. All the reagents used for preparation of the electrolyte solutions were of analytical grade. The volume of an electrolyte solution poured to the electrochemical cell was about 20 mL. Each measurement was carried out at room temperature (around 20 °C) while not stirring the electrolytes. LSV and CP measurements were carried out using an electrochemical measurement system (Hokuto Denko Co. Ltd.; HZ-3000). In LSV, a potential sweep was performed from a rest potential to the potential for hydrogen evolution at the rate of 1 mV s^{-1}. In CP, the current density was usually set at 1.0 mA cm^{-2}. The electrochemical measurements were started within 10 s after the immersion of each sample into the electrolyte solution. It should be noted that the reduction procedure should be conducted as quickly as possible after the sample is immersed in SAE. Otherwise copper oxides and/or hydroxide may be formed on the copper surface by the immersion of the sample for over 20 s.[17]

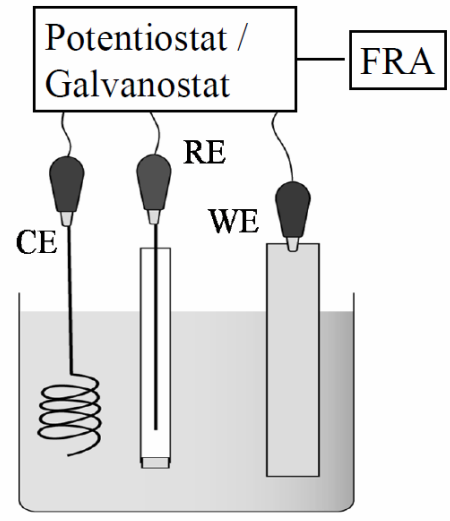

Figure 2.1 Schematic representation of the measuring system.

EIS measurements were performed by using the HZ-3000 system equipped with a frequency response analyzer (FRA; NF Co., model FRA5080). Prior to each EIS measurement, a CP measurement with −1.0 mA was performed for 3 min so that the sample electrode was kept at the reduction potential for Cu_2O or CuO. Then an ac current modulation of 0.1 mA was superimposed on the dc current of −1.0 mA at frequencies from 10 kHz to 50 mHz, and the ac voltage response was analyzed by the frequency analyzer. Commercially available software, ZSimpWin (Princeton Applied Research), was used for modeling of the obtained impedance data. This software utilizes the "downhill simplex method" based on a trial-and-error method to find the best fit for a given set of data and the chosen equivalent circuit. The parameters providing the closest fit to a model are obtained by minimizing the statistical function defined as the sum of the squares of the residuals.

2.2.3. XRD measurements

The copper oxide films were characterized by XRD on a Philips X'Pert-Pro system using

Cu-Kα radiation (45 kV-40 mA) with a grazing incident angle of 1 degree. In the geometry, crystalline thin films with a thickness of less than 100 nm are detectable. Figure 2.2 shows the XRD data for three standard samples.

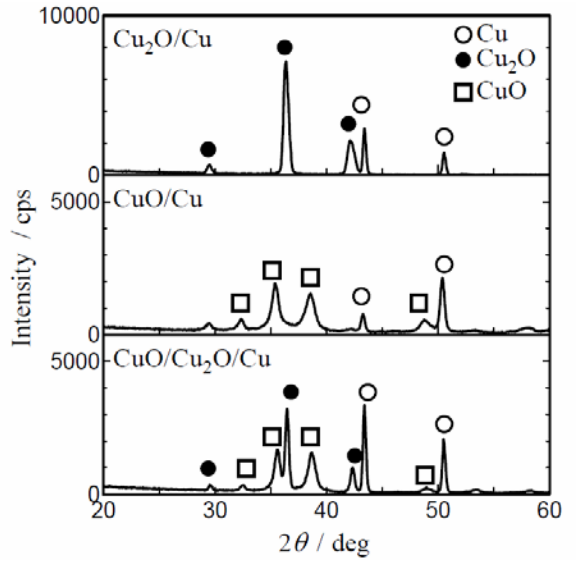

Figure 2.2 XRD patterns for three standard samples.

2.2.4. Oxygen analysis

An oxygen analyzer (Horiba Co. Ltd. ; EMGA-650W) was used to determine oxygen in a Cu_2O/Cu sample (10 cm lengths, ca. 0.34 g) and a CuO/Cu sample (0.5 cm × 1.0 cm, *ca*. 0.34 g). These samples were put into a sample container made of carbon and then heated in He at 2300 °C for 75 s. Evolved oxygen in the heating process transforms to CO by reacting with carbon. CO is determined by infrared absorption technique. This method is called "inert gas fusion analysis".

2.3. Results and Discussion

2.3.1. Influences of supporting electrolytes

Enough separation of the reduction potentials of Cu_2O and CuO could be achieved in SAE as a supporting electrolyte.[18] Figure 2.3A shows current–potential curves obtained by LSV with SAE

for three standard samples. As clearly demonstrated in the figure, CuO is firstly reduced, prior to the reduction of Cu_2O. It should be noted here that the LSV measurements were made without deaeration of the electrolyte, because the voltammograms are not entirely changed by deaeration. The reduction current of dissolved oxygen appears to be very low compared with the reduction currents of the copper oxides. Thus, a highly selective determination of Cu_2O and CuO can be performed using SAE. On the other hand, when 0.1 M KCl is used, no clear separation was found as shown in Fig. 2.3B.

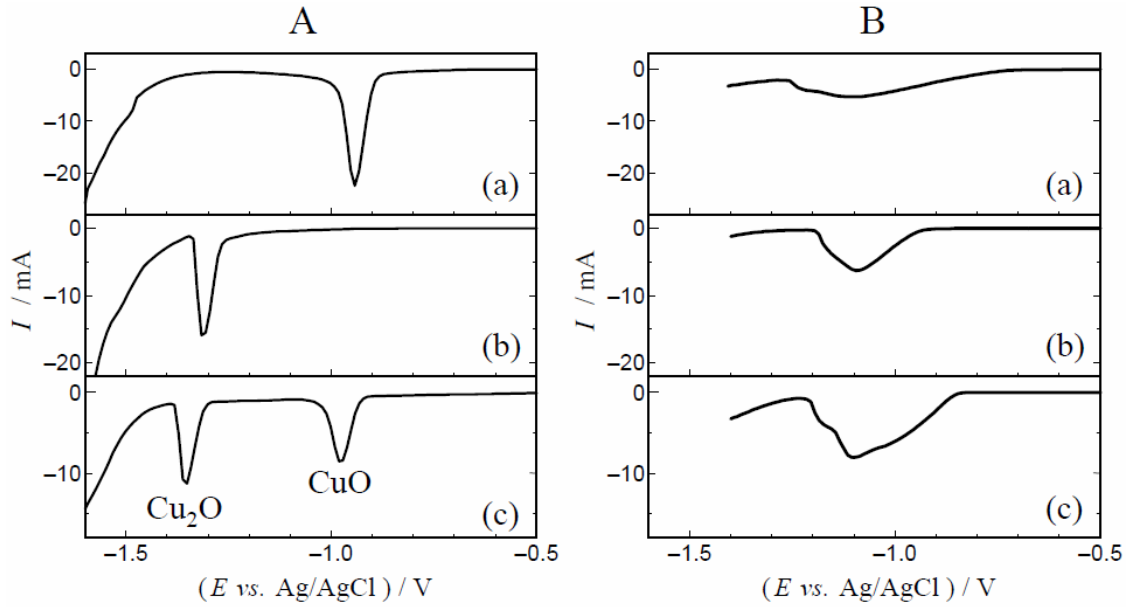

Figure 2.3 Current–potential curves recorded by LSV for (a) Cu_2O/Cu, (b) CuO/Cu, and (c) CuO/Cu_2O/Cu samples. Measurement area: 1.0 cm^2. Electrolyte solution: (A) SAE and (B) 0.1 M KCl. Scan rate: 1 mV s^{-1}.

The potential–time curves obtained by CP for CuO/Cu_2O/Cu samples in different electrolytes are shown in Fig. 2.4. As shown in panel (c), two distinct potential plateaus were observed when SAE was used. The first and second plateaus should correspond to the reduction of CuO and Cu_2O, respectively. The third potential plateau is due to hydrogen evolution. When using 0.1 M KCl (in panel (a)), however, two reduction processes for CuO and Cu_2O appeared to occur at similar

potentials. Thus, the two reduction peaks in LSV and the two potential plateaus in CP were overlapped with each other, as shown in panel (c) of Fig. 2.3B and in panel (a) of Fig. 2.4 respectively. It was thus difficult to determine the two copper oxides separately for a sample such as a $CuO/Cu_2O/Cu$ sample with a relatively thick layer, *i.e.*, about 1 μm.

When 1 M KOH was used, two reduction potential plateaus were observed as shown in panel (b) of Fig. 2.4, but their separation was worse than that when SAE was used. The second reduction potential for 1 M KOH was more negative than that for 0.1 M KCl, but only slightly more negative than that for SAE. In contrast, however, the second reduction potential was considerably shifted to a lower potential when using SAE.

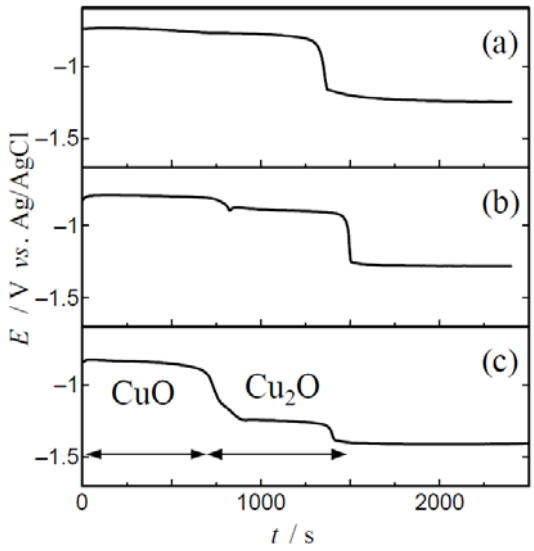

Figure 2.4 Potential–time curves recorded by CP for $CuO/Cu_2O/Cu$ standard samples in different electrolyte solutions: (a) 0.1 M KCl, (b) 1 M KOH and (c) SAE. Measurement area: 1.0 cm^2. Current density: –1.0 mA cm^{-2}.

2.3.2. Quantitative capability of the voltammetry using SAE

On the basis of the results shown in Fig. 2.3A, it can be considered that each oxide is reduced according to:

$$Cu_2O + H_2O + 2e^- \rightarrow 2Cu + 2OH^- \quad (2.1)$$

$$CuO + H_2O + 2e^- \rightarrow Cu + 2OH^- \quad (2.2)$$

Thus, CuO as well as Cu_2O is reduced to metal Cu in one step. If CuO was reduced in two steps, *i.e.*, *via* the intermediate Cu_2O, a reduction peak for Cu_2O would be observed in the voltammogram for CuO in panel (a) of Fig. 2.3A. The mass (W; in kg m^{-2}) of each oxide layer can be calculated from each peak area, *i.e.*, the quantity of electricity (Q in C) required for the reduction of the oxide layer

$$W = MQ/(nFS) \quad (2.3)$$

where M is the molecular weight of oxide in kg mol^{-1}, n is the number of electrons required for the reduction of one molecule of oxide ($n = 2$ for both Cu_2O and CuO), F is the Faraday constant, and S is the surface area of the copper sample in meters squared. If we assume that the oxide density (ρ in 10^3 kg m^{-3}) is equal to the theoretical one (*i.e.*, 6.04 and 6.315 for Cu_2O and CuO, respectively), W can be converted to the average thickness of the oxide layer (d in m)

$$d = 10^3 W/\rho \quad (2.4)$$

As mentioned above, the mass and average thickness of an oxide layer can be estimated from the area of the reduction peak. However, it was pointed out that the calculated values do not necessarily correspond to actual ones.[19] In order to investigate the quantitative capability of the voltammetry using SAE, an inert gas fusion analysis was applied for determining the amounts of oxygen in Cu_2O/Cu and CuO/Cu samples.[14] As shown in Table 2.1, converted values to the weights of Cu_2O and CuO gave close agreement with those obtained by voltammetry. For the precise calculation of peak areas, "double sweep cyclic voltammetry" (DSCV)[18] was employed, in which the voltage scan was repeated twice. By subtracting the current on the 2nd scan from that on the 1st scan, the influence of hydrogen evolution can be effectively compensated and then the net current for the reduction of oxide films may be obtained in a more accurate manner.

Table 2.1 Determination of copper oxides by two different methods.

	$Cu_2O/10^{-2}$ kg m^{-2}			$CuO/10^{-2}$ kg m^{-2}		
Method	Mean	σ[1)]	RSD[2)]	Mean	σ[1)]	RSD[2)]
DSCV	1.67	0.06	3.5	3.70	0.26	7.0
GAS[3)]	1.68	0.04	2.5	3.61	0.15	4.3

1) Standard deviation, n = 5

2) Relative Standard Deviation / %

3) Inert Gas Fusion Analysis

2.3.3. Effect of Li^+ ions

There are two principal factors related to the advantages of SAE: *i.e.*, (1) Li^+ ions and (2) high alkalinity.[20] In this section, the effect of Li^+ ions will be described.

Figure 2.5 shows potential−time curves recorded by CP for Cu_2O/Cu, CuO/Cu, and CuO/Cu_2O/Cu samples in three different electrolyte solutions: 1 M KOH, 1 M NaOH, and 1 M LiOH. If an oxide-free copper surface is dedicated to the CP measurement, the measured potential should immediately shift to the hydrogen evolution potential (ca. −1.3 V). For the CuO/Cu_2O/Cu sample in panel (c) of Fig. 2.5B, two distinct potential plateaus were observed when 1 M LiOH was used. The first and second plateaus should correspond to the reductions of CuO and Cu_2O, respectively. This was supported by the data for the Cu_2O/Cu and CuO/Cu samples, which are shown in panel (c) of Fig. 2.5A. The final potential plateau observed for every measurement is due to hydrogen evolution. When 1 M KOH or 1 M NaOH was used, two reduction potential plateaus were observed as shown in panels (a) and (b) of Fig. 2.5B; however, their separation was worse than that observed when 1 M LiOH was used.

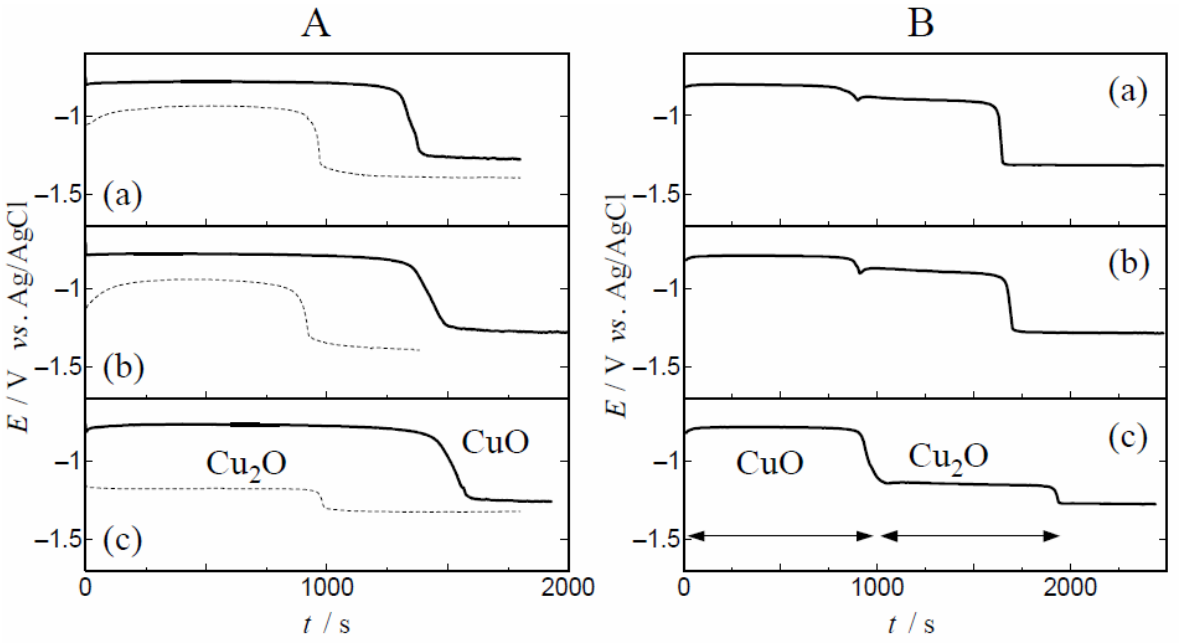

Figure 2.5 Potential–time curves recorded by CP for (A) Cu_2O/Cu and CuO/Cu samples, and (B) CuO/Cu_2O/Cu samples in three solutions of hydroxides: (a) 1 M KOH, (b) 1 M NaOH and (c) 1 M LiOH. Measurement area: 1.0 cm^2. Current density: –1.0 mA cm^{-2}.

Figure 2.6 shows the electrochemical impedances for the reductions of the CuO/Cu and Cu_2O/Cu samples in 1 M KOH, 1 M NaOH, or 1 M LiOH. In every case, a large semi-circle appeared in the upper part of the complex plane, indicating the contribution from the double-layer capacitance (C_{dl}). The diameter of the semi-circle in the high-frequency range can be recognized as the charge-transfer resistance (R_{ct}) for the reduction of copper oxides. As also shown in Fig. 2.6, a characteristic inductive loop was observed in the low-frequency range for most measurements. This loop probably indicates the existence of some reaction intermediate. Analogous inductive loops were reported for the Faradaic impedances of the dissolution of Fe in sulfuric acid[21] and the electrocrystallization of Ni or Co.[22]

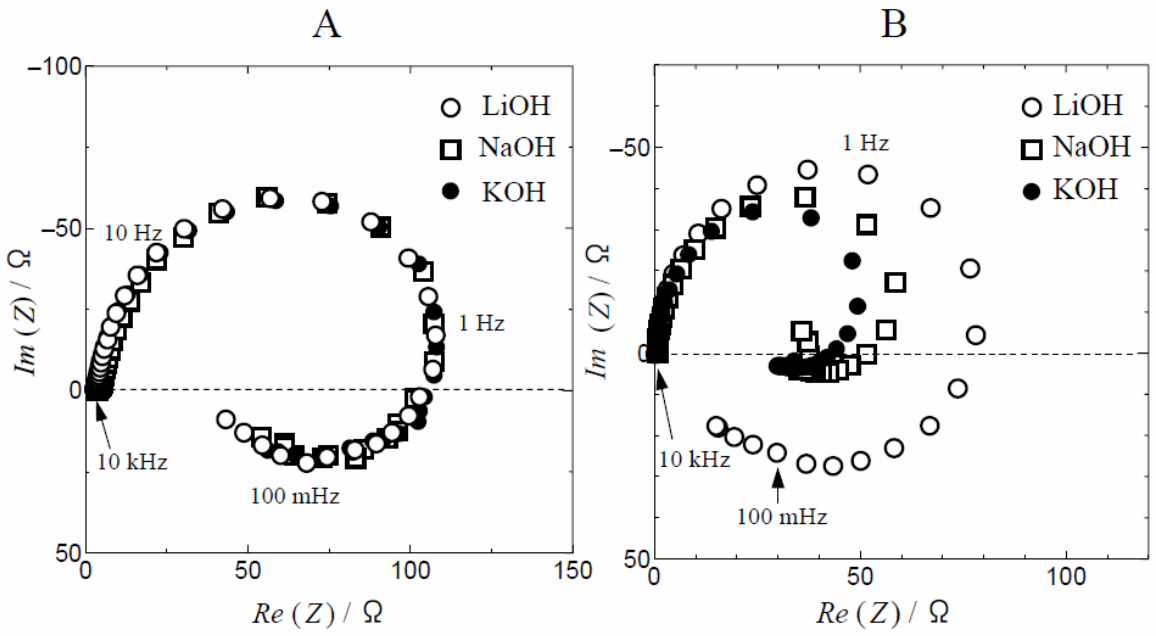

Figure 2.6 Electrochemical impedances of (A) the CuO/Cu sample and (B) the Cu_2O/Cu sample in 1 M LiOH, 1 M NaOH, and 1 M KOH. Dc current: –1.0 mA. Ac current: 0.1 mA.

As seen in Fig. 2.6A, the electrochemical impedance of the CuO/Cu sample is hardly affected by the kind of alkali hydroxide as the supporting electrolyte. This result is in harmony with the CP data shown in Fig. 2.5A. On the other hand, the impedance of the Cu_2O/Cu sample (Fig. 2.6B) was strongly affected by the kind of alkali hydroxide. The diameter of the capacitive loop (*i.e.*, R_{ct}) was the largest for LiOH and decreased in the order of LiOH > NaOH > KOH. Thus, it was shown that Li^+ ions had an increasing effect on R_{ct}, *i.e.*, an inhibitory effect on the reduction of Cu_2O. The inductive loop was also most prominent for LiOH and rather ambiguous for NaOH and KOH. Similar results showing the specific Li^+-ion effect on the Cu_2O reduction were obtained when LiCl, NaCl, and KCl were used for the supporting electrolytes (data not shown).

Figure 2.7 shows (A) the potential–time curves of the CuO/Cu_2O/Cu sample and (B) the electrochemical impedance of the Cu_2O/Cu samples, which were obtained in five different concentrations of LiOH (0.1–2 M).

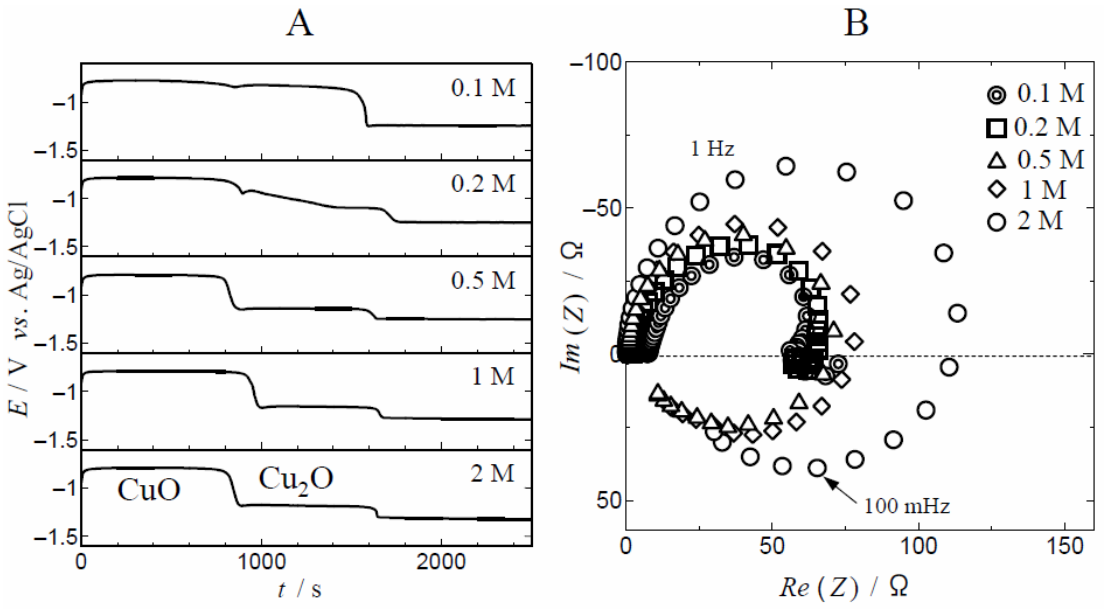

Figure 2.7 (A) Potential–time curves (at –1.0 mA) and (B) electrochemical impedance (dc current: –1.0 mA; ac current: 0.1 mA) for the Cu_2O/CuO sample in different concentrations (0.1 – 2 M) of LiOH.

As seen in Fig. 2.7A, the transition from the first potential plateau to the second one became clear when the LiOH concentration was above 0.2 M. The first plateau due to the reduction of CuO was not greatly dependent on the LiOH concentration, but the second plateau due to the reduction of Cu_2O was significantly shifted to lower potentials with increase in LiOH concentration. As shown in Fig. 2.7B, the diameter of the capacitive loop in the high frequency range was increased with increase in LiOH concentration, particularly in the region above 1 M. On the other hand, the inductive loop in the low frequency range appeared distinctly when the LiOH concentration was higher than 0.5 M.

2.3.4. Effect of alkalinity

The effect of alkalinity was also investigated. Figure 2.8 shows (A) the potential–time curves of the CuO/Cu_2O/Cu sample and (B) the electrochemical impedance of the Cu_2O/Cu samples, which were obtained in four different concentrations of KOH (1–10 M). As seen in Fig. 2.8A, the

second plateau, namely, the reduction potential of Cu_2O was shifted to lower potentials with increase in KOH concentration. Because the first plateau, namely, the reduction potential of CuO, was shifted only slightly to lower potentials, a sufficient separation between the two plateaus was achieved for KOH concentrations >6 M. Although this dependence is apparently similar to that observed for LiOH (Fig. 2.7A), much higher concentrations were required for KOH to achieve a good separation between the two plateaus. This was the case for the electrochemical impedances shown in Figs. 2.7B and 2.8B. As seen in Fig. 2.8B, both the capacitive and inductive loops became much larger when the KOH concentration was increased above 6 M.

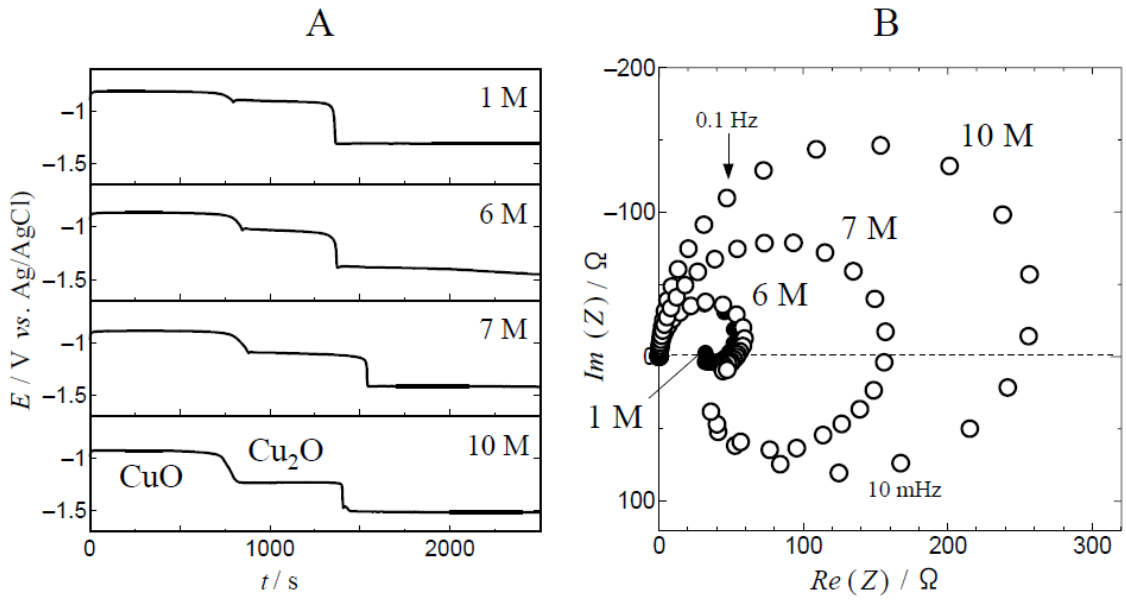

Figure 2.8 (A) Potential–time curves (at –1.0 mA) and (B) electrochemical impedance (dc current: –1.0 mA; ac current: 0.1 mA) for the Cu_2O/CuO sample in different concentrations (1 – 10 M) of KOH.

2.3.5. Simulation of the impedance data

As described above, the electrochemical impedances for the reductions of CuO and Cu_2O showed not only a capacitive but also an inductive loop in the complex plane under certain conditions. These characteristics of the electrochemical impedance are analogous to those of the

reported faradaic impedances.[21,22] By consulting the literatures, we assumed an equivalent circuit shown in Fig. 2.9 for the reductions of copper oxides. As shown in Fig. 2.9, the equivalent circuit involves a faradaic impedance (Z_F), which is connected to C_{dl} in parallel and to R_{sol} in series. Then, Z_F consists of R_{ct} in parallel with the series connection of a faradaic resistance (ρ) and a self-inductance (L):

$$\frac{1}{Z_f} = \frac{1}{R_{ct}} + \frac{1}{\rho + j\omega L} \tag{2.5}$$

where $\omega = 2\pi f$ (f being frequency). The overall impedance of the electrochemical cell can be written as

$$Z = R_{sol} + \left(\frac{1}{Z_F} + j\omega C_{dl} \right)^{-1} \tag{2.6}$$

Using Eqs. (2.5) and (2.6), non-linear least squares curve fitting was performed for the impedance data shown above. As an example, the electrochemical impedance for the Cu_2O/Cu sample in 1 M LiOH is shown in Fig. 2.10. As can be seen in the figure, the simulated or calculated plots fitted well to the measured plots. The parameters, C_{dl}, R_{sol}, R_{ct}, ρ, and L, were then evaluated as adjusting parameters, being shown in Table 2.2.[20] Similar analyses with the equivalent circuit in Fig. 2.10 could be performed also for the impedance data under other conditions. The parameters obtained for the Cu_2O/Cu sample in different concentrations of LiOH and KOH are summarized in Table 2.2. As expected, R_{sol} became smaller with increase in electrolyte concentration. Also, C_{dl} tended to increase with electrolyte concentration. The extremely high values of C_{dl} (= 2 mF cm^{-2}) seemed to be associated with the higher electrolyte concentrations and the roughness of the electrode surfaces.

The increases in R_{ct} with increases in the concentrations of LiOH and KOH correspond to the expansion of the capacitive loop.[20] Regarding the parameters ρ and L, they exhibited abnormal values (shown in parentheses) for lower concentrations of LiOH or KOH, where the inductive loop in the complex plane was ambiguous. However, the values of ρ and L were increased with

LiOH concentration (>0.2 M) and KOH concentration (>6 M). These dependences should correspond to the appearance of an inductive loop at higher alkali-hydroxide concentrations. The inductive loop suggests the existence of an intermediate species (a possible candidate being CuOH[23]). The specific inhibitory effect of Li^+ ions on Cu_2O reduction might be explained by a possible stabilization of CuOH by Li^+ ions.

$$Cu_2O + H_2O \rightarrow 2CuOH \quad (2.7)$$

$$2CuOH + 2e^- \rightarrow 2Cu + 2OH^- \quad (2.8)$$

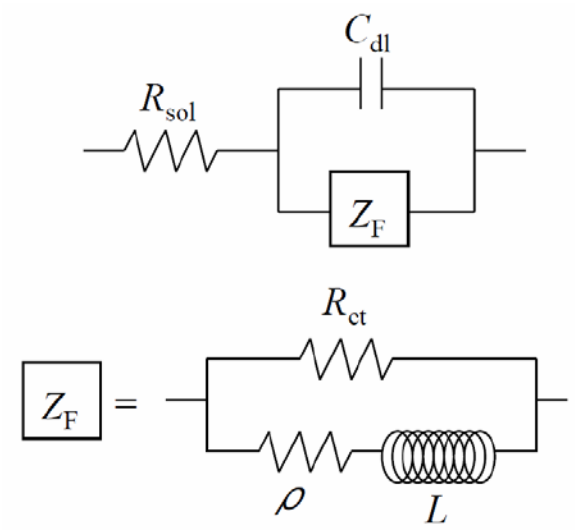

Figure 2.9 Equivalent circuit of the electrode impedance.

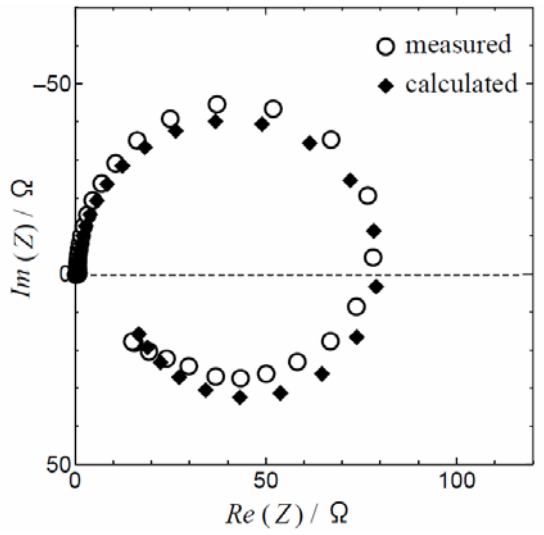

Figure 2.10 Electrochemical impedance of the Cu_2O/Cu sample in 1 M LiOH. Open circles and solid diamonds show the measured and calculated values, respectively. Dc current: –1.0 mA; ac current: 0.1 mA.

Table 2.2 Comparison of the parameters of electrode impedance for the reduction of Cu_2O in different concentrations of LiOH and KOH

Electrolyte	Parameters				
	C_{dl} / mF	R_{sol} / Ω	R_{ct} / Ω	ρ /Ω	L / H
0.1 M LiOH	0.68	9.8	66	(156)	(21)
0.2 M LiOH	0.99	2.5	70	(291)	(235)
0.5 M LiOH	2.0	1.3	73	9.2	48
1.0 M LiOH	2.0	0.8	81	14	73
2.0 M LiOH	2.0	0.5	121	31	167
1.0 M KOH	0.64	0.9	78	(54)	(4.2)
6.0 M KOH	0.68	0.3	82	(99)	(270)
7.0 M KOH	0.85	0.3	248	38	227
10 M KOH	1.2	0.2	270	59	424

For the case of LiOH (Fig. 2.7B), however, the capacitive and inductive loops were increased markedly at much lower LiOH concentrations (>0.2 M) than KOH (>6 M). Thus, although the solution alkalinity has a definite effect on the suppression of the Cu_2O reduction, Li^+ ions should have a specific effect on it. Taking into consideration the solubility of reagents, we have then proposed SAE with the composition of 6 M KOH + 1 M LiOH, as the best electrolyte for the selective determination of copper oxides.

References

1. H.A. Miley, *J. Am. Chem. Soc.*, **59,** 2626 (1937).
2. W. E. Campbell and U. B. Thomas, *Trans. Electrochem. Soc.*, **76**, 303(1939).
3. R. H. Lambert and D. J. Trevoy, *J. Electrochem. Soc.*, **105**, 18 (1958).
4. T. Koizumi, S. Furuya, T. Kuroha, and Y. Maeda, *J. Jpn. Copp. Brass. Res. Assoc.*, **15**, 211 (1976).
5. S. J. Krumbein, B. Newell, and V. Pascucci, *J. Test. Eval.*, **17**, 357 (1989).
6. *Standard Specification for Hot-Rolled Copper Redraw Rod for Electrical Purposes*, ASTM B49-50, ASTM, Philadelphia, PA (1990).
7. B. I. Rickett and J. H. Payer, *J. Electrochem. Soc.*, **142**, 3713 (1995).
8. H. Pops and D. R. Hennessy, *Wire J. Int.*, **10**, 50 (1977).
9. Z. Peide, R. P. M. Procter, W. A. Grant, and V. Ashworth, *Nucl. Instrum. Methods Phys. Res.*, **209/210**, 841 (1983).
10. J. Y. Malvault, J. Lopitaux, D. Delahaye, and M. Lenglet, *J. Appl. Electrochem.*, **25**, 841 (1995).
11. R. L. Deutscher and R. Woods, *J. Appl. Electrochem.*, **16**, 413 (1986).
12. M. Lenglet, K. Kartouni, and D. Delahaye, *J. Appl. Electrochem.*, **21**, 697 (1991).
13. M. Pourbaix, " Atlas of Electrochemical Equilibria inAqueous Solutions, 2nd English ed.",

p.387, NACE, Houston, TX (1974).

14. S. Nakayama, M. Shibata, T. Notoya and T. Osakai, *Bunseki Kagaku*, **51**, 1145 (2002).
15. Y. Fujita, K. Ikeshima, US patent 6383254 (2002).
16. S. Nakayama, T. Kaji, T. Notoya and T. Osakai, *J. Electrochem. Soc.*, **154**, C1 (2007).
17. S. Nakayama, T. Notoya and T. Osakai, *Journal of the JRICu*, **49**, 273 (2010).
18. S. Nakayama, A. Kimura, M. Shibata, S. Kuwabata and T. Osakai, *J. Electrochem. Soc.*, 148, B467 (**2001**).
19. Y. Y. Su and R. M. Shemenski, *Surf. Interface Anal.*, **40,** 1183 (2008).
20. S. Nakayama, T. Kaji, T. Notoya and T. Osakai, *Electrochim. Acta*, **53**, 3493 (2008).
21. I. Epelboin, M. Keddam, *J. Electrochem. Soc.* **117**, 1052 (1970).
22. I. Epelboin, R. Wiart, *J. Electrochem. Soc.* **118**, 1577 (1971).
23. M. D. Bharadwaj and J. C. Yang, *Scripta Mater.*, **44**, 2557 (2001).

Chapter 3. Reduction Order of Copper Oxides

3.1. Introduction

There were conflicting views regarding the reduction order of copper oxides.[1,2] Miley[3] and other authors[4–7] claimed that the reduction of Cu_2O first occurred, followed by the reduction of CuO. This view is the basis of the standard method[8] proposed by the American Society for Testing and Materials (ASTM), however no convincing evidence has been presented. On the other hand, several authors proposed that CuO was reduced prior to the reduction of Cu_2O.[9–13] Su and Marek[12] proposed a two-step reaction mechanism in which the reduction of CuO to Cu_2O occurs first, and the generated Cu_2O and also the originally existing Cu_2O are then reduced simultaneously. The reports claiming the two different reduction orders of copper oxides are listed in Table 3.1. CP was employed in the studies shown in the table, except for our study[14] in which double sweep cyclic voltammetry was employed.

Table 3.1 List of reports claiming the two different reduction orders of copper oxides.

$Cu_2O \rightarrow CuO$	$CuO \rightarrow Cu_2O$
Miley[3] (1937)	Mills and Evans[9] (1956)
Koizumi *et al.*[4] (1976)	Booker and Salim[10] (1972)
Pops and Hennessy[5] (1977)	Peide *et al.*[11] (1983)
Krumbein *et al.*[6] (1989)	Su and Marek[12] (1994)
Rickett and Payer[7] (1995)	Nakayama *et al.*[14] (2001)[a]
ASTM[8] (2008)	Reid *et al.*[13] (2008)

a. This study was only performed using double sweep cyclic voltammetry. CP was employed in other studies.

In 2003, a sub-committee on the cathodic reduction of copper-oxide films was constituted in the Japan Society of Corrosion Engineering (JSCE). I attended the committee as a member. The

committee performed round-robin experiments to determine which mechanism is valid in the cathodic reduction of Cu-duplex air-formed thin oxide films. In the committee's report,[1] it was concluded that in CP measurements with 0.1 M KCl as the supporting electrolyte, CuO was first reduced to Cu in one step, followed by the reduction of Cu_2O. This conclusion was drawn from XPS measurements. However, the copper samples used were composed of a rather thin and not fully identified oxide layer. Then, we carried out an independent study on the reduction order by using copper samples with a thicker and fully identified oxide layer.

3.2. Experimental

3.2.1. Samples

Three different samples of Cu-duplex oxide film were prepared: (1) a $CuO/Cu_2O/Cu$ standard sample (denoted as Sample A), (2) an oxygen-free copper sheet (0.50 mm thick; JIS H 3100 C1020P-1/2H) immersed in 0.5 M NaOH at 30 °C for 32 h (Sample B), and (3) the same oxygen-free copper sheet as that for the preparation of Sample B, but was heated at 300 °C for 20 min (Sample C).

In electrochemical measurements for the samples, the surface area to be tested was usually 1.0 cm^2.

3.2.2. Electrochemical measurements

LSV and CP measurements were carried out in the same manner as shown in § 2.2.2. In LSV, a potential sweep was applied from a rest potential to the potential for hydrogen evolution at the rate of 1.0 or 10 mV s^{-1}. In CP, the current density was usually set at 1.0 mA cm^{-2}.

3.2.3. XRD measurements

XRD measurements were carried out in the same manner as shown in § 2.2.3.

3.2.4. Scanning ion microscopic observation

Cross sections of the oxide films were observed by scanning ion microscopy (SIM) with an FEI FIB2000 system. The specimens were first mechanically cut and polished with a 0.3 μm Al_2O_3 lapping film. Then, in order to protect the oxide films, the polished specimens were coated with *ca.* 1-μm-thick Pt in the FIB2000 system by using the ion-beam-assisted chemical vapor deposition (CVD) technique. Finally, the specimens were further polished by a focused ion beam (FIB) of Ga at 30 keV and used for SIM observation.

3.3. Results and Discussion

3.3.1. Reduction order of Cu_2O and CuO in CP

To determine which oxide is first reduced in 0.1 M KCl, the LSV method with SAE was applied to the samples prepared by partial and complete cathodic reduction of Sample A in 0.1 M KCl.

Prior to this, the same method was applied to the samples prepared by CP measurements in SAE. Figure 3.1A shows the potential–time curve recorded by CP for Sample A. The current–potential curve recorded by LSV for the non-reduced sample, which had two distinct reduction peaks, is shown in panel (a) of Fig. 3.1B. However, the first reduction peak for CuO disappeared, as shown in panel (b) of Fig. 3.1B, for the sample that was prepared by partial reduction, that is, by interrupting the CP measurement after the first reduction process was terminated. When the CP measurement was completed, both reduction peaks disappeared, as shown in panel (c) of Fig. 3.1B. Thus, CuO is first reduced at a higher potential and then Cu_2O is reduced at a lower potential in SAE.

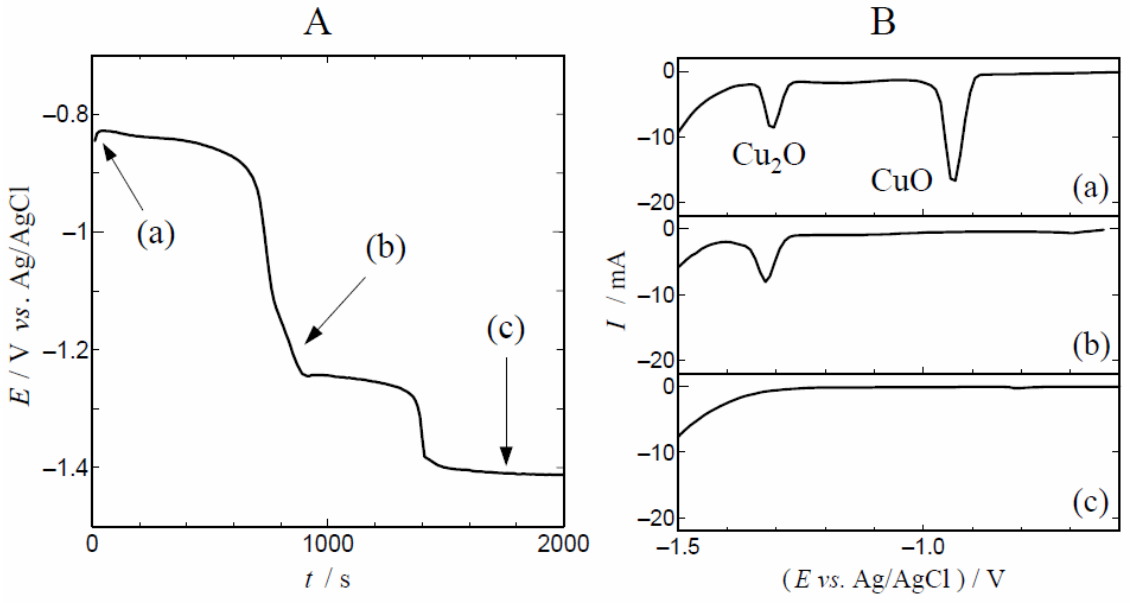

Figure 3.1 The potential–time curve of Sample A recorded by CP with SAE at –1.0 mA cm^{-2}. Panels (a), (b), and (c) in B show the current–potential curves recorded by LSV with SAE at 1.0 mV s^{-1} for the samples (a) not reduced, (b) partially reduced, and (c) completely reduced by the CP measurement shown in A.

A similar procedure was then used for CP measurements with 0.1 M KCl. The results are shown in Fig. 3.2. The potential–time curve (as in panel (a) of Fig. 2.4) had no distinct potential jump indicating the termination of the first reduction process. Then, considering the potential–time curve in Fig. 3.1A, the CP measurement was interrupted at 800 s, and the partially reduced sample was submitted to LSV measurement using SAE. As shown in panel (b) of Fig. 3.2B, the reduction peak of CuO was lowered but did not disappear. The reduction peak of Cu_2O was slightly lowered. The sample after the CP measurement gave no reduction peaks for the copper oxides, as shown in panel (c) of Fig. 3.2B. These results clearly show that the reduction of CuO also occurs first, followed by the reduction of Cu_2O, in 0.1 M KCl. However, it was revealed that the reductions of Cu_2O and CuO occurred simultaneously, to a greater or lesser extent, in a neutral solution such as 0.1 M KCl. It should also be noted that CuO was reduced to metal Cu in one step, *i.e.*, not *via* Cu_2O, because the reduction peak of Cu_2O was not increased accompanying the reduction of CuO,

as shown in panels (a) and (b) of Fig 3.2. This result disagrees with the previous two-step reaction mechanism.[12,15]

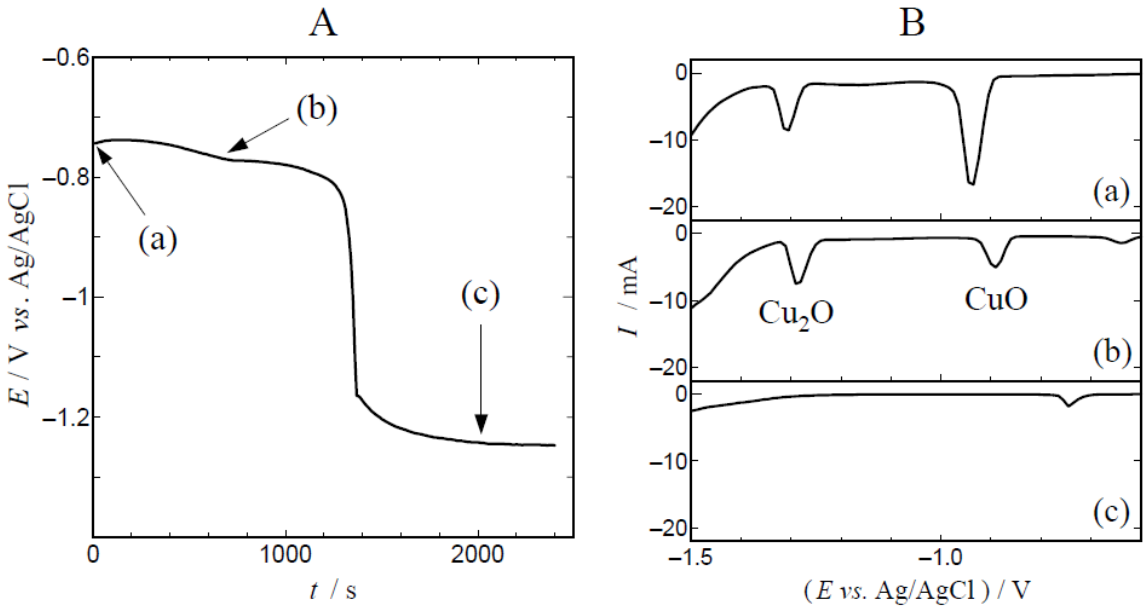

Figure 3.2 Potential–time curve of Sample A recorded by CP with 0.1 M KCl at –1.0 mA cm^{-2}. Panels (a), (b), and (c) in B show the current–potential curves recorded by LSV with SAE at 1.0 mV s^{-1} for the samples (a) not reduced, (b) partially reduced, and (c) completely reduced by the CP measurement shown in A.

In order to confirm the above conclusion, an additional experiment was carried out. Panel (b) of Fig. 3.3 shows XRD patterns for the samples prepared by reducing Sample A in 0.1 M KCl to different extents, *i.e.*, by interrupting CP measurement at different times as shown in panel (a) of Fig. 3.3. As clearly shown by the change in the XRD patterns, CuO was found to be reduced more preferentially than Cu_2O. However, the reduction peaks of the two oxides in LSV or the corresponding potential plateaus in CP are not well separated for 0.1 M KCl, as shown above; this might have caused confusion in the understanding of the order of reduction for the oxides.

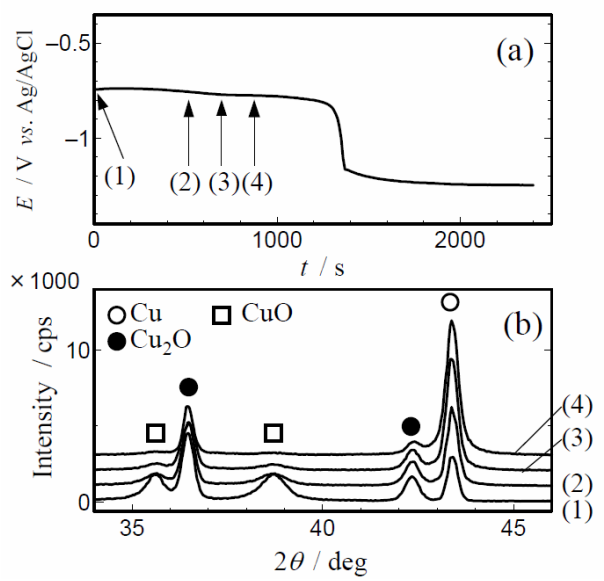

Figure 3.3 (a) Potential–time curve of Sample A recorded by CP with 0.1 M KCl at –1.0 mA cm^{-2} and (b) XRD patterns for the samples (1) not reduced and (2)-(4) partially reduced by interrupting the CP measurement at different times indicated by the arrows in the upper panel (a).

From above discussions, one can conclude that the outer CuO layer generated on the Cu_2O layer in Sample A should be preferentially reduced to metal Cu to give a Cu/Cu_2O/Cu sandwich structure, which was predicted in the previous paper.[14] This structure was actually observed in the sample prepared by a partial reduction of Sample A in 0.1 M KCl. Figure 3.4 shows FIB/SIM images of the cross sections of sample A and its partially and completely reduced samples. As seen in Fig. 3.4B, a well-developed Cu layer was formed on the Cu_2O layer to show the sandwich structure. When the CP measurement was performed until hydrogen evolution was observed, the remaining oxide layer of Cu_2O was also converted to Cu, as shown in Fig. 3.4C.

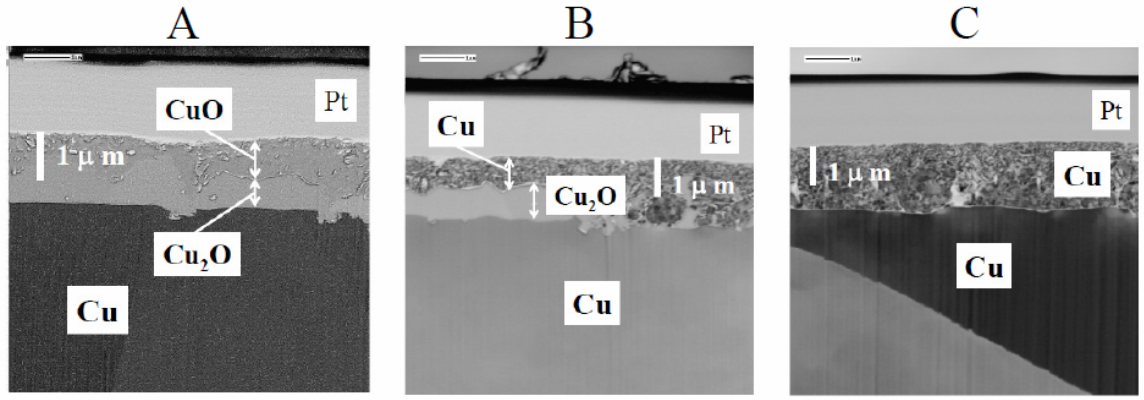

Figure 3.4 FIB/SIM images of the cross sections of samples prepared by (A) without reduction, (B) partial and (C) complete reductions of Sample A by CP measurements with 0.1 M KCl (the respective samples correspond to those shown by (a), (b), and (c) in Fig. 3.2).

3.3.2. Other samples prepared in different ways

To confirm the above conclusion deduced from the experiments with Sample A, similar experiments to those shown in Fig. 3.2 were performed with Samples B and C, which were prepared in different ways described above. Figure 3.5 shows XRD patterns for Samples A, B, and C. As seen in the figure, the XRD patterns demonstrated the existence of both Cu_2O and CuO for each sample, although no well-developed peaks for Cu_2O and CuO were obtained for Sample C, probably because of the lower crystallinity of the oxide layers.

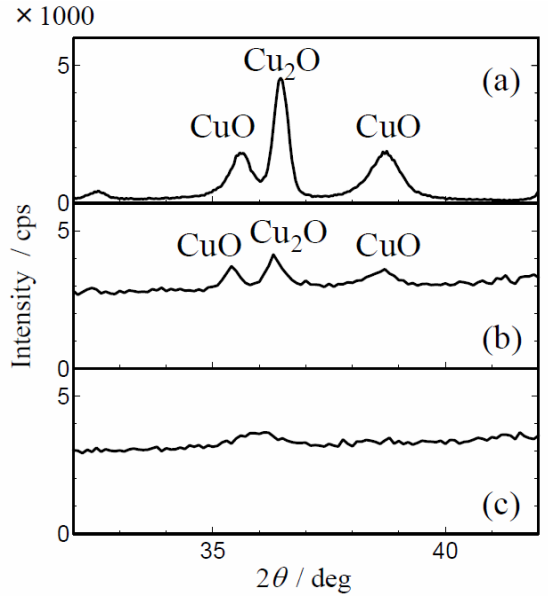

Figure 3.5 XRD patterns for (a) Sample A, (b) Sample B, and (c) Sample C.

The results for Sample B are shown in Fig. 3.6. The CP measurement with 0.1 M KCl was interrupted at two different times, and the partially reduced samples as well as the non-reduced sample were submitted to LSV measurements with SAE. As shown in Fig. 3.6, CuO was more preferentially reduced than Cu_2O, in a similar manner as shown for Sample A in Fig. 3.2. This was also confirmed by XRD measurements, though the data are not shown. The thicknesses of the oxide layers for Sample B were estimated from the peak areas in panel (a) of Fig. 3.6B, to be *ca.* 0.8 μm for CuO and *ca.* 0.5 μm for Cu_2O, the total thickness being *ca.* 1.3 μm.

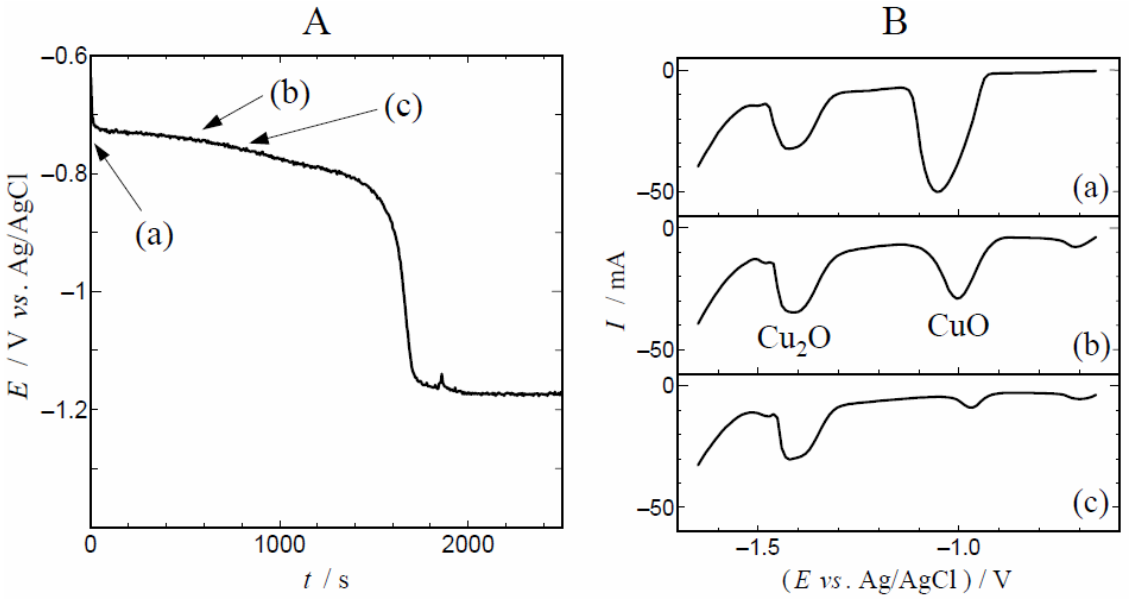

Figure 3.6 Potential–time curve of Sample B recorded by CP with 0.1 M KCl at –1.0 mA cm^{-2}. Panels (a), (b), and (c) in B show the current–potential curves recorded by LSV with SAE at 10 mV s^{-1} for the samples (a) not reduced and (b), (c) partially reduced by interrupting the CP measurement shown in A at the times indicated by arrows.

Similar results were also obtained for Sample C, as shown in Fig. 3.7. Although the reduction peak for Cu_2O was somewhat ill-defined, the reduction of CuO occurs first in the same way as for Samples A and B. The thicknesses of the oxide layers were estimated from panel (a) of Fig. 3.7B, to be *ca.* 0.2 μm for CuO and *ca.* 0.4 μm for Cu_2O (the total thickness being 0.6 μm).

Thus, it was confirmed that CuO was first reduced, followed by the reduction of Cu_2O in 0.1 M KCl, for copper oxide films having the thickness of about 1 μm.

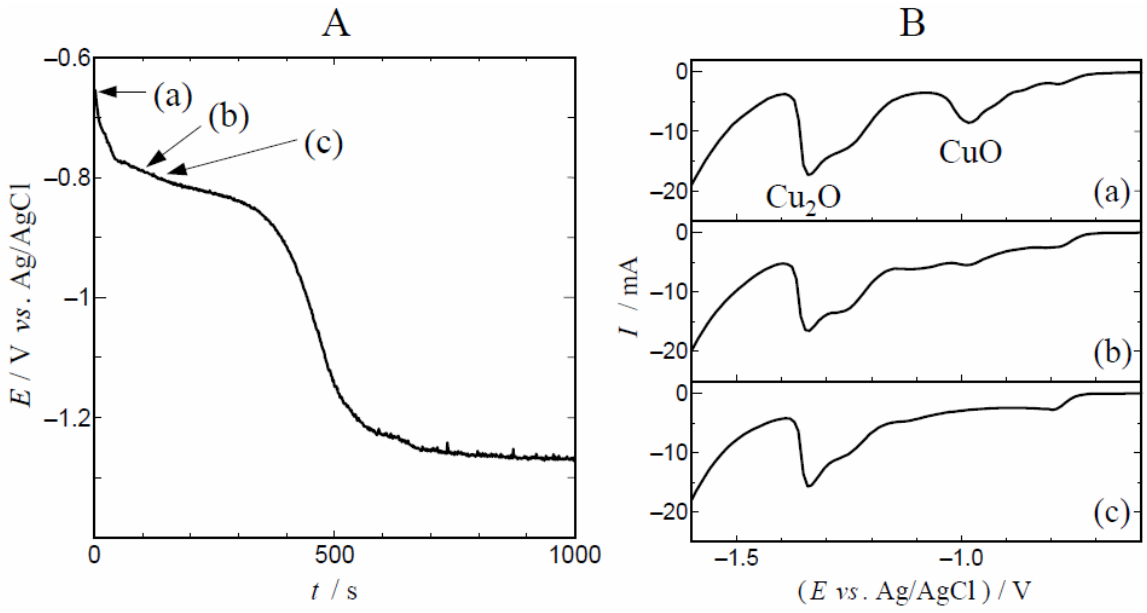

Figure 3.7 Potential–time curves of Sample C recorded by CP with 0.1 M KCl at –1.0 mA cm^{-2}. Panels (a), (b), and (c) in B show the current–potential curves recorded by LSV with 6 M KOH + 1 M LiOH at 10 mV s^{-1} for the samples (a) not reduced and (b), (c) partially reduced by interrupting the CP measurement shown in A at the times indicated by arrows.

References

1. M. Seo, Y. Ishikawa, M. Kodaira, A. Sugimoto, S. Nakayama, M. Watanabe, S. Furuya, R. Minamitani, Y. Miyata, A. Nishikata and T. Notoya, *Corros. Sci.*, **47**, 2079 (2005).
2. Y.Y. Su, S. Nakayama and T. Osakai, *Corros. Rev.*, **29**, 51 (2011).
3. H.A. Miley, *J. Am. Chem. Soc.*, **59**, 2626 (1937).
4. T. Koizumi, S. Furuya, T. Kuroha and Y. Maeda, *Journal of the JRICu*, **15**, 211 (1976).
5. H. Pops and D.R. Hennessy, *Wire J. Int.*, **10**, 50 (1977).
6. S.J. Krumbein, B. Newell and V. Pascucci. *J. Test. Eval.*, **17**, 357 (1989).
7. B.I. Rickett and J. H. Payer, *J. Electrochem. Soc.*, **142**, 3713 (1995).
8. "*Standard Specification for Hot-Rolled Copper Redraw Rod for Electrical Purposes*", ASTM

B49-08, 2008, ASTM, Philadelphia, PA.

9. T. Mills and U.R. Evans, *J. Chem. Soc., Part 2*, 2182 (1956).
10. C.J.L. Booker and M. Salim, *Nature, Phys. Sci.*, **239**, 62 (1972).
11. Z. Peide, R.P.M. Procter, W.A. Grant and V. Ashworth, *Nucl. Instrum. Meth.*, **209/210**, 841 (1983).
12. Y.Y. Su and M. Marek , *J. Electrochem. Soc.*, **141**, 940 (1994).
13. M. Reid, J. Punch, L.F. Garfias-Mesias, K. Shannon, S. Belochapkine and D.A. Tanner, *J. Electrochem. Soc.*, **155**, C147 (2008).
14. S. Nakayama, A. Kimura, M. Shibata, S. Kuwabata and T. Osakai, *J. Electrochem. Soc.*, **148**, B467 (2001).
15. R. L. Deutscher and R. Woods, *J. Appl. Electrochem.*, **16**, 413 (1986).

Chapter 4. Analysis of Other Corrosion Products

4.1 Introduction

So far, mainly two oxides (*i.e.*, Cu_2O and CuO) have been submitted for analysis by conventional electrochemical methods. In this chapter are described further applications of the developed method to copper corrosion products other than oxides, which include sulfides, hydroxide, and "patina".

In the 1930s, a chemical state analysis of copper oxide films by CP was reported,[1] and was also applied for the analysis of chalcocite, Cu_2S,[2,3] which is the most common corrosion product in the sulfides formed on copper. Like copper oxides,[2] copper sulfides cause various discolorations of copper surfaces, depending on the thickness of the sulfide layer.[4] It should be added that the supporting electrolytes used in the CP measurements for copper sulfides were also neutral or weak alkaline electrolytes such as 0.1 M KCl.

On the other hand, copper hydroxides and "patina" have not been analyzed by the conventional electrochemical methods. "Patina" is the general term for "rusts of copper" produced by long-term exposure to air,[5,6] and it refers to basic copper minerals, which include basic copper chlorides, sulfides, carbonates, and others.

4.2. Experimental

4.2.1. Samples

Powder reagents of Cu_2O (99.5%), CuO (99.9%), $Cu(OH)_2$ (95%) , Cu_2S (99.5%), CuS （99.5%） , $CuSO_4{\cdot}5H_2O$ (99.5%), and basic copper sulfate (Antlerite; $Cu_3(SO_4)(OH)_4$), all supplied from Wako Pure Chemicals Ltd., Osaka, were used as standard samples. Each sample was mixed with a carbon paste consisting of graphite powder and paraffin oil (both available from ALS Co., Ltd., Tokyo) with the weight ratio of 1 : 5. The resulting mixture (*ca.* 0.5 mg) was spread over a glassy carbon disc electrode (3 mm-ϕ) to prepare a carbon paste electrode.[7] A glassy carbon

electrode for special use was also purchased from ALS Co. Ltd.

For investigating the sulfidizing behavior of copper, an oxide-free copper plate (JIS H 3100 C1020P; 99.99% purity) of 0.5 mm thick was used, which was etched in advance with HCl. Copper sulfides (mainly Cu_2S) formed on the copper plate by immersing in a 5 mM Na_2S solution at 25 °C for 1 min to 8 h. The formed Cu_2S/Cu sample as well as the standard sample of Cu_2O/Cu[8] was subjected to the analysis by electrochemical impedance spectroscopy (EIS).

An enamel copper wire (2 mm-ϕ), which was discolored in the manufacturing process in my company (SEI Ltd.), was also analyzed by LSV.

4.2.2. Electrochemical measurements

LSV and CV measurements were carried out in the same manner as those shown in § 2.2.2. The surface area of copper samples, excluding powder samples, was normalized to 1.0 cm^2. The supporting electrolyte was SAE or 0.1 M KCl. The potential sweep rate in the CV and LSV measurements was 10 or 1 mV s^{-1}. For each EIS measurement, a dc current of –1 mA was applied in advance to the sample for 3 min, so that the electrode potential became the reduction potential of copper sulfides or oxides. Thereafter, while applying the dc current, an EIS measurement was performed with an ac current of 0.1 mA, by changing the frequency from 10 kHz to 50 mHz, with 10 points per decade.[9] In all electrochemical measurement, no deaeration was applied to the electrolyte solution.

4.2.3. XRD measurements

XRD measurements were made in a wide-angle mode (θ–2θ) and in a thin-film mode. From the measurements in the former and latter modes, information was acquired for a surface layer of the thickness of 20 μm and of a few micrometers, respectively. A RINT1500 diffractometer from Rigaku Corp., Tokyo, was used in a focused beam mode for the former measurement, with a Cu source operated with voltage 50 kV and current 200 mA. On the other hand, X′ Pert-Pro from

Philips was used for the latter measurement, operated with a parallel beam optical system under the condition of detecting a diffraction signal from a 100-nm-thick crystalline thin film. In this measurement, a probe X-ray beam incident angle was taken to be 1°. The X-ray source was Cu operated with voltage 45 kV and current 40 mA.

4.2.4. ICP-OES

Sulfidizing treatment for an oxygen-free copper plate was done by immersing the test piece with exposed surface 2 × 2 cm in 5 mM Na_2S at 30 °C for 4 h or 8 h. The test piece was then immersed in a mixed solution consisting of HNO_3 10 mL, H_2O_2 0.5 mL, and distilled water 10 mL at 150 °C held in an autoclave and left for 3 h. Thereafter, the resulting solution was diluted using a volumetric flask, and the S level in the solution was measured using an SPS 1200 VR inductively coupled plasma-optical emission spectroscopy (ICP-OES) analyzer from Seiko Instruments Inc.

4.3. Results and Discussion

4.3.1. Reduction behavior of powder standard samples in different electrolytes

Figure 4.1 shows current–potential curves for standard powder samples (*i.e.,* Cu_2O, CuO, $Cu(OH)_2$, Cu_2S, and CuS) in two different types of electrolytes, *i.e.*, SAE and 0.1 M KCl. Although these samples are commercially available, it is unable to use the powder samples directly for an electrochemical measurement. Then, carbon-paste electrodes were prepared by mixing a carbon paste with a powder sample and sticking the paste onto a glassy carbon disk electrode.[7] As shown in Fig. 4.1A, the reduction peaks for Cu_2O and CuO were clearly separated in SAE. However, in 0.1 M KCl (Fig. 4.1B), the peak separation between Cu_2O and CuO was not clear. In SAE, the peak of $Cu(OH)_2$ emerged at a slightly positive potential than that of CuO, corresponding to the thermodynamic order. Appreciable tailing toward the less positive potential side was observed for the reduction peak of $Cu(OH)_2$. This tailing appeared to suggest the occurrence of slow subsequent reactions, although the details remain unknown. Also note in Fig. 4.1B that the reduction peak of

$Cu(OH)_2$ shifted toward an extremely negative potential in 0.1 M KCl. On the other hand, the reduction peak for Cu_2S was not greatly affected by the type of electrolyte. In the voltammogram for a CuS powder sample, two peaks of comparable areas were detected in both the electrolytes.[10]

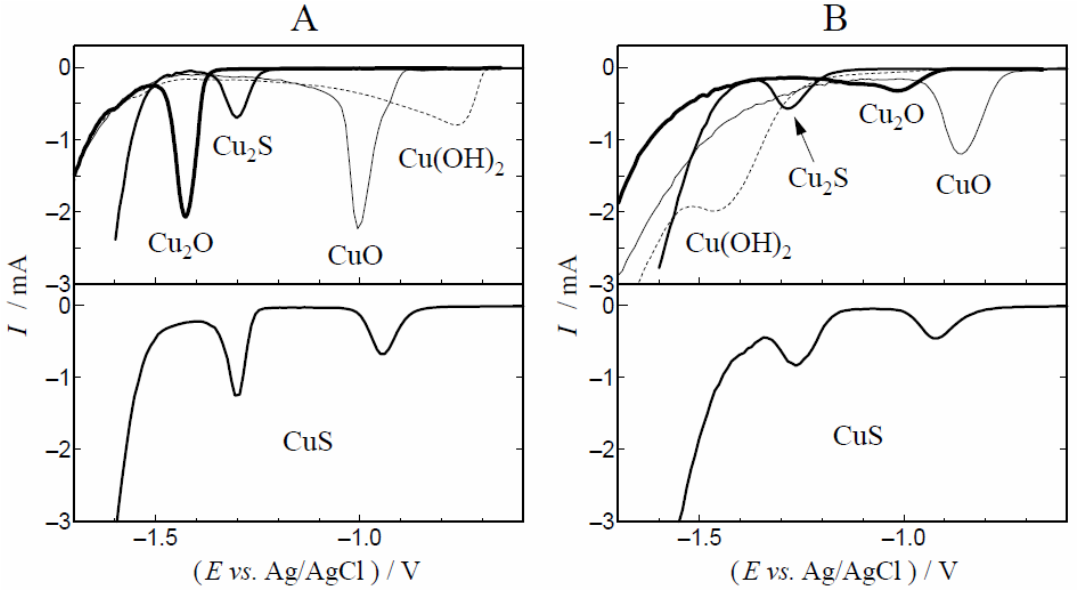

Figure 4.1 Current–potential curves recorded by LSV for standard powder samples. Electrolyte solutions: (A) SAE and (B) 0.1 M KCl. Scan rate: 10 mV s^{-1}.

The peak for Cu_2S emerged at a slightly higher potential than that of Cu_2O in SAE. The order of the observed reduction potentials is inconsistent with that predicted from thermodynamic consideration. The redox reactions for Cu_2O and Cu_2S are expressed as follows:

$$Cu_2O + H_2O + 2e^- \rightarrow 2Cu + 2OH^- \qquad E° = -0.365 \text{ V} \qquad (4.1)$$

$$Cu_2S + 2e^- \rightarrow 2Cu + S^{2-} \qquad E° = -0.898 \text{ V} \qquad (4.2)$$

where $E°$ is the standard electrode potential vs. SHE. The value of $E°$ in Reaction (4.2) is more negative than that in Reaction (4.1), and is close to the peak potential (–1.0 V vs. SHE) for the reduction of Cu_2S in LSV (Fig. 4.1). On the other hand, the equilibrium electrode potential (E) for

Reaction (4.1) depends on pH as follows:[11]

$$E = 0.471 - 0.0591\ \text{pH} \quad \text{(in V vs. SHE)} \tag{4.3}$$

Even when pH = 15 for SAE, E should be more positive than the $E°$ value for Reaction (4.2) (*i.e.*, –0.898 V). Actually, however, Cu_2S was reduced prior to Cu_2O. Thus, the reduction order of Cu_2O and Cu_2S in SAE cannot be elucidated based on thermodynamics, suggesting that some kinetic factors should be involved in the reduction mechanisms. On the other hand, it was reported that Cu_2O was reduced prior to Cu_2S in neutral or weak alkaline electrolytes.[2,3] This reduction order is the same as that observed in 0.1 M KCl (see Fig. 4.1B).

4.3.2. Analysis of Copper Sulfides

Sulfidizing reaction of copper

Researchers in the field of copper corrosion have been interested not only in copper oxides but also in copper sulfides. Recently, some corrosion tests have been carried out using mixed flowing gases containing H_2S.[12,13]

Sulfidation of copper requires some sulfur sources. Copper sulfides can form easily on copper surfaces when copper plates are exposed to an atmosphere containing H_2S gas[2,14,15] or immersed in a solution containing sulfide ions.[16] In this study, copper plates were first ground using a SiC #2000 abrasive-coated paper and then immersed in 5 mM Na_2S for various periods. The color of the copper surface was changed from red via blue to gray, being affected by the coherence of light.[4] Figure 4.2 shows the current potential–curves of copper plates immersed in 5 mM Na_2S for 1, 10, and 60 min. Referring to the current–potential curves in Fig. 4.1A, the peak observed at –0.8 V to –0.9 V can be ascribed to the reduction of $Cu(OH)_2$. As shown in the figure, two split cathodic peaks were observed at lower potentials and grew with increasing the treatment time. This suggested that besides $Cu(OH)_2$, at least two chemical species were formed by sulfidation of the copper plates.

Using XRD (θ–2θ), however, Cu_2S (chalcocite-M) phase was only identified with reference to the ICDD cards (00-033-0490). The main peak appearing at a more negative potential seemed to be due to the reduction of Cu_2S.

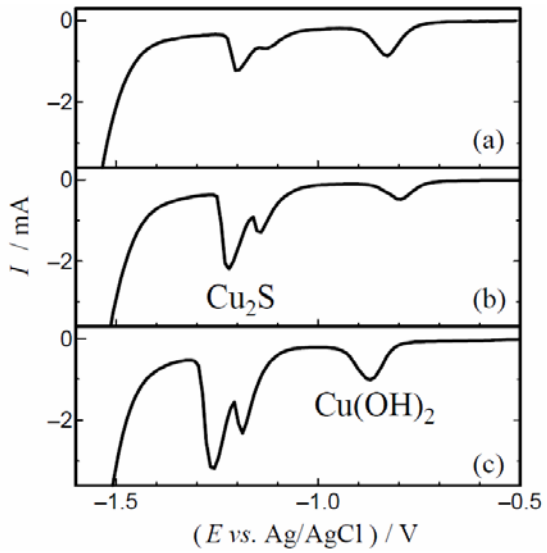

Figure 4.2 Current–potential curves recorded by LSV for the copper plates immersed in 5 mM Na_2S at 25 °C for (a) 1 min, (b) 10 min, and (c) 60 min. Electrolyte solution: SAE. Scan rate: 10 mV s^{-1}

For identifying the smaller cathodic peak appearing at a less negative potential (–1.1 to –1.2 V), two additional copper samples with thicker sulfide films were prepared by treatment with a 5 mM Na_2S solution for 4 h and 8 h. As seen in the voltammograms of Fig. 4.3A, two split cathodic peaks were obtained in a similar manner to those for the samples in Fig. 4.2. It should here be noted that the main peak at the more negative potential grew preferentially with a longer immersion time. Figure 4.3B shows the XRD pattern obtained for the sample immersed in the Na_2S solution for 8 h. To ensure acquisition of top surface XRD information, the XRD patter was obtained using the thin-film XRD technique. As shown in the figure, besides the clear diffraction peaks for Cu_2S, weak but certainly detectable peaks were obtained for a Cu_9S_5 phase (digenite: ICDD 00-009-0064).[17]. Accordingly, the smaller cathodic peak appearing at the less negative

potential may be ascribed to the reduction of Cu_9S_5. I would like to add that the reduction peak of Cu_9S_5 was consistently smaller than that of Cu_2S.

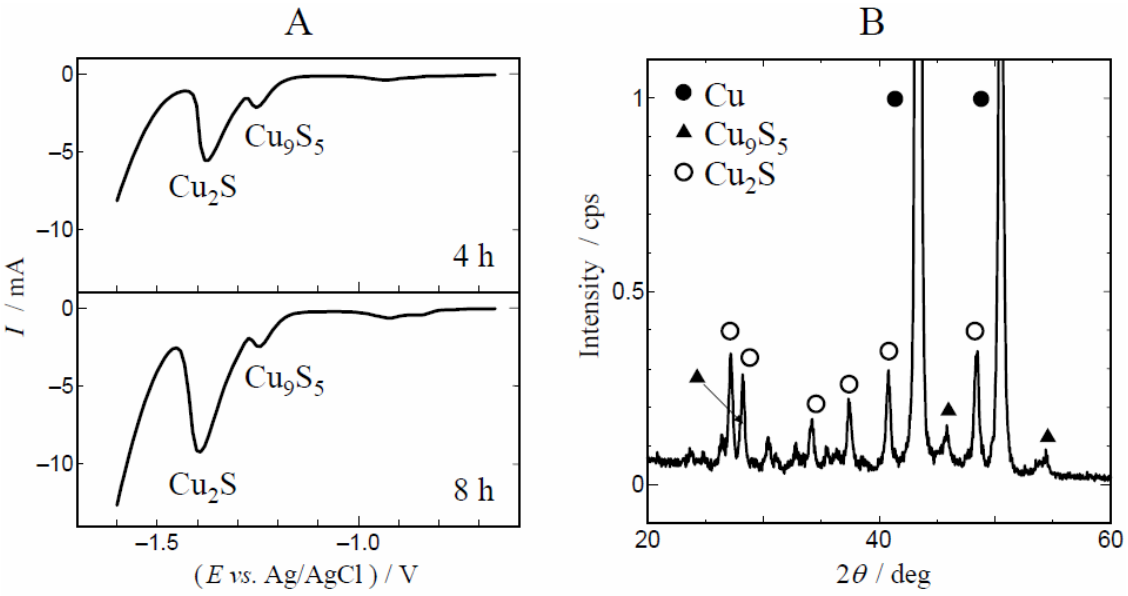

Figure 4.3 (A) Current–potential curves recorded by LSV with 6 M KOH + 1 M LiOH at 10 mV s^{-1}, and (B) XRD patterns for the copper plates immersed in 5 mM Na_2S at 25 °C for 8 h.

Reduction behavior of Cu_2S

EIS measurements were carried out for a more detailed investigation of the reduction behavior of copper sulfides (Cu_2S), which was compared with that of Cu_2O. Test samples were Cu_2O/Cu[8] and Cu_2S/Cu.[10] The latter sample was obtained by immersing a copper plate in a 5 mM Na_2S solution at 25 °C for 8 h. It is known that Cu_2S formed by the reaction of copper and S^{2-} ions in an aqueous solution.[16] Figure 4.4 shows Cole-Cole plots of the electrochemical impedance for the reduction of Cu_2O/Cu and Cu_2S/Cu in two types of electrolytes (*i.e.*, SAE and 0.1 M KCl). As seen in Fig. 4.4A, the electrochemical impedance of Cu_2O reduction depended appreciably on the type of electrolyte. In SAE, the charge transfer resistance R_{ct} (represented by the diameter of each semicircle in the high-frequency range) was incomparably greater than that in 0.1 M KCl. This suggested that the reduction of Cu_2O was strongly suppressed in SAE. In addition, an inductive loop was detected

in the low-frequency range. It is generally acknowledged that the emergence of an inductive loop suggests the presence of intermediate reaction products.[18] Meanwhile, the values of R_{ct} for Cu_2S reduction (Fig. 4.4B) were comparable in the two types of electrolytes. This behavior is compatible with the small difference in the reduction potential of Cu_2S in the two electrolytes (Fig. 4.1). Since the reduction of Cu_2O was selectively and strongly suppressed in SAE as described in § 2.3.1, the reduction order of Cu_2O and Cu_2S was inverted depending on which electrolyte was used.

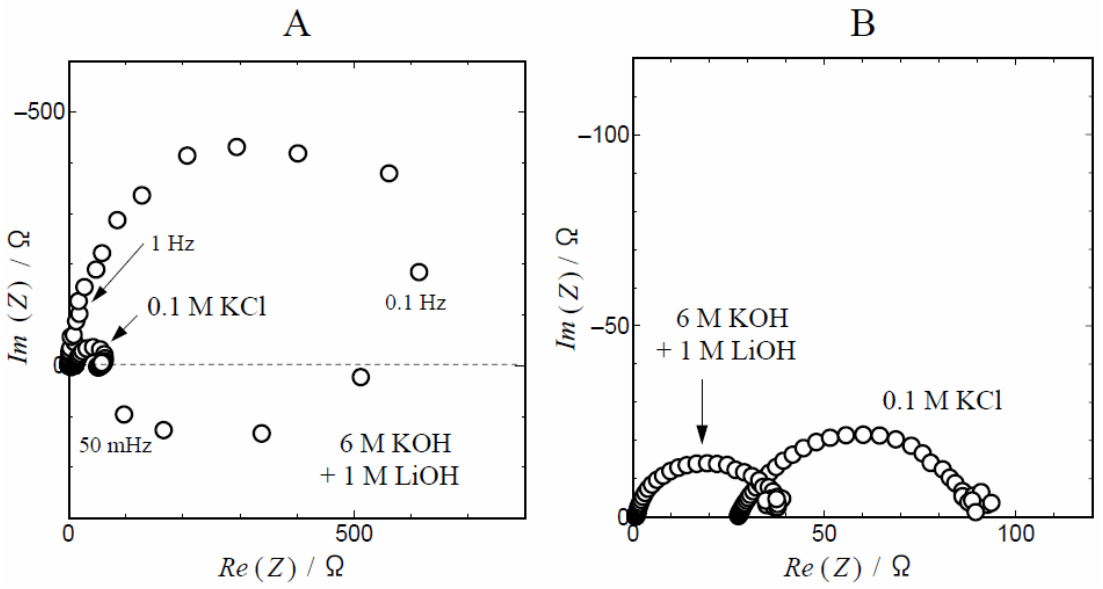

Figure 4.4 Electrochemical impedances of (A) a Cu_2O/Cu sample and (B) a Cu_2S/Cu sample. Electrolyte solutions used for each sample were SAE and 0.1 M KCl. Current density: −1.0 mA cm^{-2}. Imposed current was 0.1 mA.

Quantitative analysis for copper sulfides

As shown above, two copper sulfides including Cu_2S and Cu_9S_5 were identified for the samples tested. Cu_2S, being known as chalcocite, exists in a monoclinic form at temperatures below 103 °C and with a hexagonal form at higher temperatures. On the other hand, Cu_9S_5 (or $Cu_{1.8}S$; being known as digenite) exists in a trigonal form. Although Cu_9S_5 can also be written as "$CuS{\cdot}4Cu_2S$", this compound should exist as the crystallographic form (trigonal) distinctly different from those of CuS (hexagonal) and Cu_2S (monoclinic). This is also apparent from the

characteristic reduction peak of Cu_9S_5, which is shown in Fig. 4.3.

The reduction reactions of Cu_2S and Cu_9S_5 ($Cu_{1.8}S$) can be written as

$$Cu_2S + 2e^- \rightarrow 2Cu + S^{2-} \quad (4.4)$$

$$Cu_{1.8}S + 2e^- \rightarrow 1.8Cu + S^{2-} \quad (4.5)$$

For both reactions, two electrons are required for liberation of one sulfide ion. Therefore, using the reduction peak areas (*i.e.*, the amounts of electricity), one can evaluate the amounts of sulfur in the respective copper sulfides. Table 4.1 shows the values determined in the LSV measurements shown in Fig. 4.3(A). In Table 4.1 are also shown the total amount of sulfur in the copper sulfides, which was determined by ICP-OES. As shown in the table, the sum of the sulfur amounts in the respective sulfides, being determined by LSV, was in reasonable agreement with the total amount of sulfur determined by ICP-OES. This showed that the LSV method with SAE is useful for selective and quantitative determination of Cu_2S and Cu_9S_5 formed on copper surfaces. The average thickness of a relatively thin sulfide film estimated for the sample submitted to the LSV measurement (panel (a) in Fig. 4.2) was as small as 8 nm. Thus, the developed method enables us to estimate the thickness of a sulfide layer with nanometer-order precision.

Table 4.1 The amounts of sulfur in copper sulfides as determined for the samples in Fig. 4.3(A) by means of LSV and ICP-OES.

Time of immersion (h)	S (mg/cm^2)		
	in Cu_2S (LSV)	in Cu_9S_5 (LSV)	in both sulfides (ICP-OES)
4	0.0071	0.0019	0.0111
8	0.0184	0.0029	0.0223

Criteria for the presence and absence of sulfides

As shown in Fig. 4.1A, the reduction peaks of Cu_2O and Cu_2S in SAE emerged at nearby potentials. Accordingly, it is rather difficult to distinguish these two peaks for samples consisting comparable amounts of Cu_2O and Cu_2S, for example, for copper specimens exposed to atmosphere. Then, we studied the detailed reduction behaviors of Cu_2O and Cu_2S in SAE, while referring to the reports for their voltammetric behaviors in the presence of sulfide ion (S^{2-}) in an alkali solution.[19,20]

As a preliminary study, we recorded current–potential curves for an oxygen-free copper plate (a) without and (b) with injection of 5 mM Na_2S in SAE. The results are shown in Fig. 4.5. The potential sweep was performed from the rest potential (around –0.7 V) to −1.6 V, and then, two successive cyclic potential scans were performed between −1.6 V and the rest potential. The current–potential curve shown in panel (a) was recorded in the absence of S^{2-} in the electrolyte; under these conditions, only a cathodic current due to H_2 evolution was observed. On the other hand, in the current–potential curve shown in panel (b), which was recorded in the presence of 5 mM S^{2-} in the electrolyte, a clear anodic peak was observed on the first and second anodic scans at −1.0 V, as indicated by an arrow. On the following cathodic scans, a prominent cathodic peak was observed reproducibly at around −1.3 V, though the peak potential was slightly shifted. Referring to the thermodynamic redox potentials, we considered the observed anodic and cathodic peaks, respectively, as:

$$2Cu + S^{2-} \rightarrow Cu_2S + 2e^- \quad (4.6)$$

$$Cu_2S + 2e^- \rightarrow 2Cu + S^{2-} \quad (4.7)$$

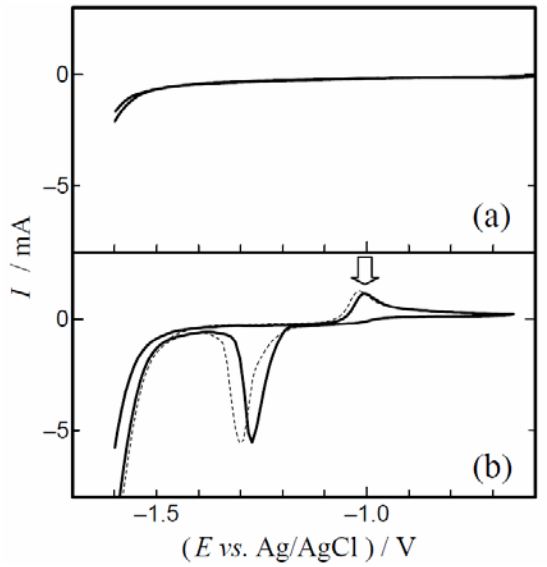

Figure 4.5 Current−potential curves recorded by CV for an oxygen-free copper plate (a) without and (b) with injection of 5 mM Na_2S in SAE. The potential was first scanned from the rest potential (around −0.7 V) to −1.6 V, and then two successive cyclic potential scans (*i.e.*, the 1st scan (solid line) and the 2nd scan (dashed line)) were performed between −1.6 V and the rest potential. Scan rate: 10 mV s^{-1}.

In the S^{2-}-containing highly alkaline electrolyte, a Cu_2S layer is thus formed by the oxidation of the base metal copper on the first anodic scan, and on the following cathodic scan, the sulfide layer is reduced to liberate S^{2-} ions into the electrolyte solution. In the voltammetric measurement shown in Fig. 4.5, a relatively high concentration of S^{2-} was present in the electrolyte, so that the anodic and cathodic current peaks were unchanged in height for the first and second cyclic potential scans.

To verify the above postulated mechanism, additional CV measurements were performed for a Cu_2S/Cu sample prepared by immersing in 5 mM Na_2S for 60 min and also a discolored enamel copper wire. In these measurements, the potential scan was performed from the initial potential to −1.6 V in the cathodic direction, followed by the anodic to the initial potential. As shown by arrows in Fig. 4.6, a weak anodic peak due to the formation of Cu_2S was observed at around −1.0 V for both the samples. The appearance of this anodic peak enabled us to make sure that there was

Cu_2S (not Cu_2O) on the surface of the copper samples. Compared with the result shown in Fig. 4.5, it seemed, from the relatively small anodic peak, that the surface concentration of S^{2-} liberated by the reduction of Cu_2S on the copper samples was lower than the added concentration (*i.e.*, 5 mM) of S^{2-} for the measurement shown in Fig. 4.5(b).

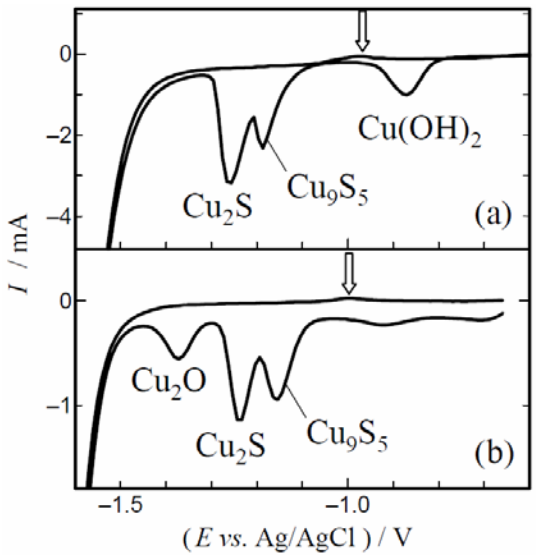

Figure 4.6 Current–potential curves recorded by CV for (a) a copper plate immersed in 5 mM Na_2S for 60 min at 25 °C and (b) a discolored enamel copper wire. Electrolyte solution: SAE. Scan rate: 10 mV s^{-1}. Arrows indicate the small anodic peak for the formation of Cu_2S on the copper surface.

4.3.3. Analysis of $Cu(OH)_2$ and Patina

So far, $Cu(OH)_2$ has not been subjected to electrochemical detection by CP or LSV. It was found that the LSV method using SAE enables detection of $Cu(OH)_2$ separately from copper oxides and sulfides, as shown in Fig. 4.1A. In SAE, $Cu(OH)_2$ gives its reduction peak at the most negative potential around –0.9 V. In 0.1 M KCl (Fig. 4.1B), however, the reduction peak of $Cu(OH)_2$ is obtained at a more negative potential, suggesting difficulty of reduction in a neutral solution.

Antlerite ($Cu_3(SO_4)(OH)_4$), which is found in nature as a mineral, is commercially available

from Wako Pure Chemical Industries. A powder sample, after being kneaded into a carbon paste, was subjected to LSV measurement with SAE. As shown in panel (a) of Fig. 4.7, a broad peak appears around –0.85 V. Since antlerite can also be shown as "$2Cu(OH)_2 \cdot CuSO_4$", powder samples of $Cu(OH)_2$ and $CuSO_4 \cdot 5H_2O$ were subjected to LSV measurement. As shown in panel (b) of Fig. 4.7, the peak of antlerite is similar to that of $Cu(OH)_2$. However, no well-defined reduction peak of $CuSO_4 \cdot 5H_2O$ was obtained because the water-soluble salt added to the carbon paste was dissolved into the electrolyte solution. By immersing the powder of antlerite in SAE for 1 h, one can see that the color of the powder has been changed from green to blue.

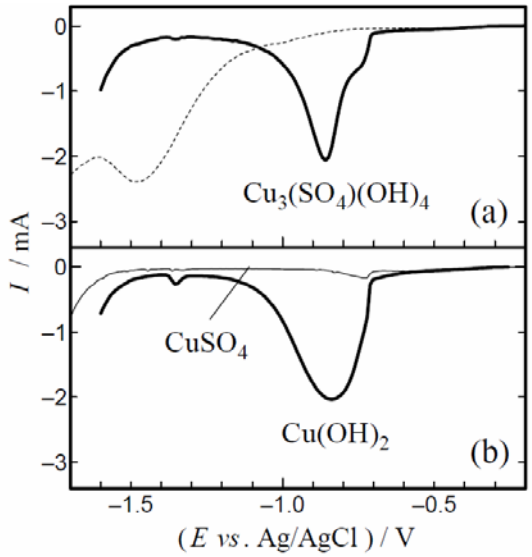

Fig. 4.7 Current–potential curves recorded by LSV for powder samples of (a) "antlerite" $\{Cu_3(SO_4)(OH)_4\}$ and (b) $Cu(OH)_2$ and $CuSO_4 \cdot 5H_2O$. Electrolyte solution: SAE and 0.1 M KCl. Scan rate: 10 mV s^{-1}.

It was confirmed from XRD patterns (Fig. 4.8) that the color change is due to the transformation of antlerite to $Cu(OH)_2$. Besides "antlerite", a basic copper carbonate, "malachite" ($Cu_2(CO_3)(OH)_2$ or $CuCO_3 \cdot Cu(OH)_2$), is also commercially available from Wako Pure Chemical Industries. Although data are not shown, the current–potential curve of malachite in SAE is similar to that of $Cu(OH)_2$. However, it is difficult for "patina" to be reduced in 0.1 M KCl. The

current–potential curve (a dotted line) of "antlerite" is shown in panel (a) of Fig. 4.7. Thus, the present results suggested the possibility of analysis of patinas using SAE.

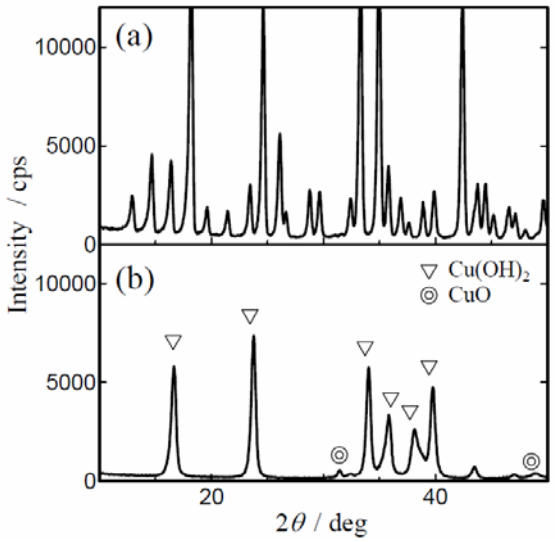

Figure 4.8 XRD patterns for antlerite (a) with no treatment and (b) after immersion in SAE for 1 h.

Figure 4.9A shows current–potential curves for an electric copper wire of 2 mm-ϕ (*ca*. 1 cm), which was wired in an air for about 20 years. As shown by the solid line, the well-defined anodic peak at –1.4 V showed the presence of Cu_2O, whereas the broad anodic peak appearing at a less negative potential showed the presence of another corrosion product(s). In order to identify the corrosion product(s), XRD measurements were performed for the wire samples not reduced and partially reduced by stopping the voltammetric potential scan at –1.2 V (see the current–potential curve shown by a dotted line in Fig. 4.9A). For the non-reduced sample shown in Fig. 4.9B(a), besides Cu_2O, two basic copper sulfides, *i.e.*, brochantite ($Cu_4SO_4(OH)_6$) and posnjakite ($Cu_4SO_4(OH)_6 \cdot H_2O$) were identified. For the partially-reduced sample shown in Fig. 4.9B(b), however, no XRD peaks for the basic copper sulfides were observed. Therefore, the broad cathodic peak at around –0.85 V may be ascribed to the reduction of basic copper sulfides. Studies are currently in progress to establish the voltammetric analysis of patinas.

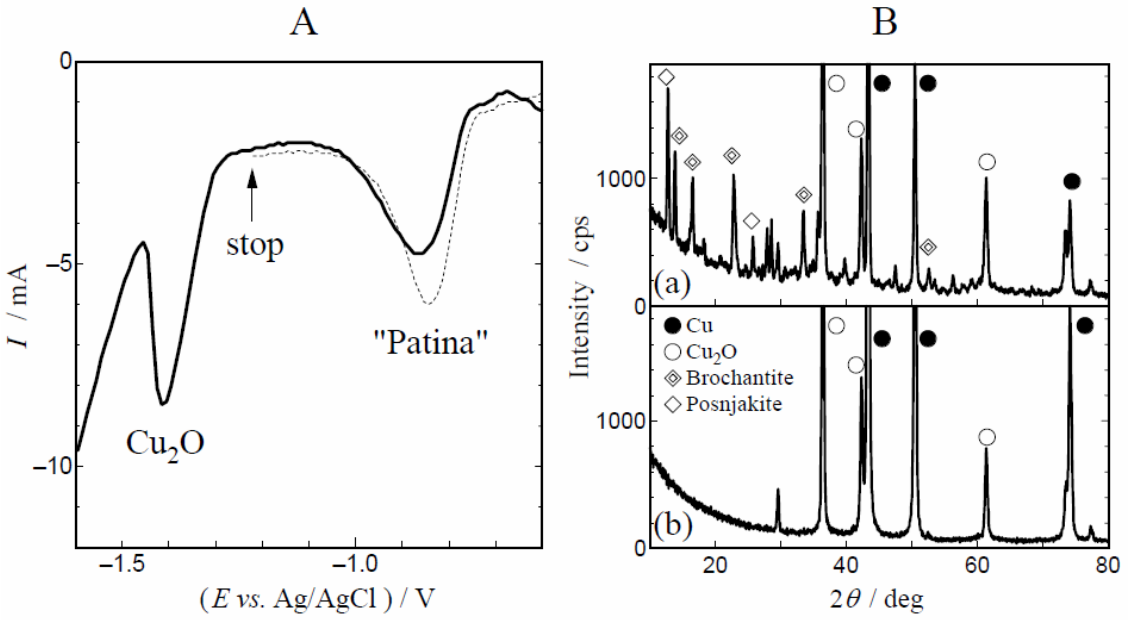

Figure 4.9 (A) Current–potential curves recorded by LSV for an electric copper wire, which was wired in an air for about 20 years. For the curve shown by a dotted line, the voltammetric scan was stopped at –1.2 V. Sweep rate: 1 mV/s. (B) XRD patterns for the wire samples (a) not reduced and (b) partially reduced by stopping the voltammetric scan as shown by the dotted line in panel (A).

References

1. H.A. Miley, *J. Am. Chem. Soc.*, **59**, 2626 (1937).
2. W.E. Campbell and U.B. Thomas, *Trans. Electrochem. Soc.*, **76**, 303 (1939).
3. J.B. Dyess and H.A. Miley, Trans. *Amer. Inst. Min. Met. Eng.*, **133**, 239 (1939).
4. S. Nakayama and T. Tokiko, *SEI Tech. Rev.*, **74**, 8 (2012).
5. T. E. Graedel, K. Nassau, and J. P. Franey, *Corros. Sci.*, **27**, 639 (1987).
6. T. E. Graedel, *Corros. Sci.*, **27**, 721 (1987).
7. S. Nakayama, M. Shibata, T. Osakai, and T. Notoya, *Journal of the JRICu*, **43**, 235 (2004).
8. S. Nakayama, M. Shibata, T. Notoya and T. Osakai, *Bunseki Kagaku*, **51**, 1145 (2002).
9. S. Nakayama, T. Kaji, T. Notoya and T. Osakai, *Electrochim. Acta*, **53**, 3493 (2008).

10. S. Nakayama, T. Kaji, T. Notoya, and T. Osakai *Zairyo-to-Kankyo*, **57**, 327 (2008), in Japanese; the English translation is available in *Corros. Eng.*, **57**, 419 (2008).
11. M. Pourbaix, Atlas of Electrochemical Equilibria in Aqueous Solutions, 2nd English ed., p.386 (1974).
12. M. Reid, J. Punch, L. F. Garfias-Mesias, K. Shannon, S. Belochapkine, and D. A. Tanner, *J. Electrochem. Soc.*, **155**, C147 (2008).
13. K. Demirkan, G. E. Derkits, Jr., D. A. Fleming, J. P. Franey, K. Hannigan, R. L. Opila, J. Punch, W. D. Reents, Jr., M. Reid, B. Wright, and C. Xu, *J. Electrochem. Soc.*, **157**, C30 (2010).
14. S. P. Sharma, *J. Electrochem. Soc.*, **127**, 21 (1980).
15. M. Watanabe, M. Tomita, and T. Ichino, *J. Electrochem. Soc.*, **149**, B97 (2002).
16. J. M. Smith, J. C. Wren, M. Odziemkowski, and D. W. Shoesmith, *J. Electrochem. Soc.*, **154**, C431 (2007).
17. G. Donnay, J. D. H. Donnay, and G. Kullerud, *Am. Mineral.*, **43**, 228 (1958).
18. I. Epelboin, M. Keddam, *J. Electrochem. Soc.*, **117**, 1052 (1970).
19. M. I. Schimmel, N. R. de Tacconi and K. Rajeshwar, *J. Electroanal. Chem.*, **453**, 187 (1998).
20. S.M. Abd El Haleem and E.E. Abd El Aal, *Corrosion*, **62**, 121 (2006).

Chapter 5. Growth Mechanism of Copper Oxides

5.1 Introduction

In the absence of such corrosive gases as H_2S, major corrosion products of copper are its oxides (*i.e.*, Cu_2O and CuO). It has been reported that in the atmosphere, Cu_2O was first formed, followed by the formation of CuO and its growth by further oxidation.[1,2] Other forms of copper oxides, including amorphous-Cu_2O (Cu_xO)[3,4] and Cu_3O_2,[5,6] have also been reported. The existence of Cu_3O_2 was identified by the XRD technique.[5] However, there is no clear basis for the existence of Cu_xO. Besides these copper oxides, copper hydroxides (mainly $Cu(OH)_2$) may be formed in air. To my knowledge, however, there have been no reports on the role of $Cu(OH)_2$ in the corrosion process of copper.

In this chapter, the developed voltammetric method with SAE was applied to a mechanistic study of copper corrosion in the atmosphere. We particularly focused on the role of $Cu(OH)_2$ in the corrosion process, which had not been adequately studied. It was previously reported that the reduction peak of $Cu(OH)_2$ appeared at a lower potential than that of Cu_xO; however, the identification was ambiguous.[7] In voltammetric studies of copper electrodes in alkaline solutions,[8,9] $Cu(OH)_2$ was found to form on the copper electrode by sweeping the potential to those more anodic than the formation potential of CuO. It was also reported that in the anodic oxidation of copper in 0.1 M NaOH, the passive layer structure on copper was changed in the order of Cu/Cu_2O, $Cu/Cu_2O/Cu(OH)_2$, $Cu/Cu_2O/CuO/Cu(OH)_2$, and $Cu/Cu_2O/CuO$, depending on the oxidation potential.[10] Thus, there have been a few reports on electrochemical behaviors of $Cu(OH)_2$ on metal copper, but the role of $Cu(OH)_2$ in the atmospheric corrosion has not been clearly established. In this study, we successfully employed the voltammetric method with SAE to clarify the significant role of $Cu(OH)_2$ in the corrosion process of copper in the atmosphere.

5.2. Experimental

5.2.1. Samples

Oxide-free copper plates (0.5 mm in thickness; JIS H 3100 C1020P; 99.99% purity) were used for corrosion tests in the atmosphere. Each copper plate was cut into 20 mm × 50 mm pieces and then etched in 6 M hydrochloric acid, followed by rinsing successively with distilled water and ethanol. Various samples of copper oxide films were prepared on the copper plates by (1) heating in a temperature/humidity-controlled chamber at 80 °C and RH 90%, (2) heating in a temperature-controlled oven at 300 °C, and (3) immersing in 0.5 M NaOH at 30 °C. At one end of a treated copper plate, a definite area (2.0 cm^2) was kept as a working electrode surface by masking the other areas with PTFE seal tape.

5.2.2. Electrochemical measurements

LSV measurements were carried out in the same manner as shown in § 2.2.2. A potential sweep was performed from a rest potential to the potential for hydrogen evolution at the rate of 10 or 100 mV s^{-1}. The electrolyte solutions used were 0.1 M KCl and SAE.

5.2.3. XRD measurements

A Philips X'Pert-Pro XRD system using Cu Kα radiation (45 kV, 40 mA) was used to characterize the oxides formed on copper plates by measuring powder XRD patterns (in θ-2θ scan).

5.3. Results and Discussion

5.3.1. Atmospheric corrosion tests

Figure 5.1 shows current–potential curves recorded by LSV for copper plates heated at 80°C and RH 90%.[11] The current–potential curves shown in panel (a) of Fig. 5.1A are partially zoomed in Fig. 5.1B. As shown in Fig. 5.1B, a current peak is observed around –0.7 V for the sample treated for a short period (*i.e.*, 10 min). Referring to the results for standard powder samples in Fig.

4.1A, one may ascribe the observed peak to the reduction of $Cu(OH)_2$. It was thus considered that $Cu(OH)_2$ is firstly formed on an uncorroded surface in the initial stage of atmospheric corrosion. As also shown in Fig. 5.1A, with increase in the treatment period from 10 min to 1 h, the reduction peak grew and shifted to more negative potentials up to around –1.0 V. This suggested that $Cu(OH)_2$ was converted to CuO in the corrosion process (also see Fig. 5.1A). Prolonging the treatment period for more than 1 h, however, no longer enhanced the peak of CuO. Instead, the reduction peak of Cu_2O appeared at –1.3 to –1.4 V and then grew with increase in the treatment time up to at least 1 day. As shown in panel (b) of Fig. 5.1A, the CuO layer formed in the early stage of corrosion grew again after the growth of the Cu_2O layer stopped. Although the oxidation rate was relatively low, a similar growth behavior of copper oxides was observed when copper plates were heated at 50 °C and RH 90% (data not shown).[11]

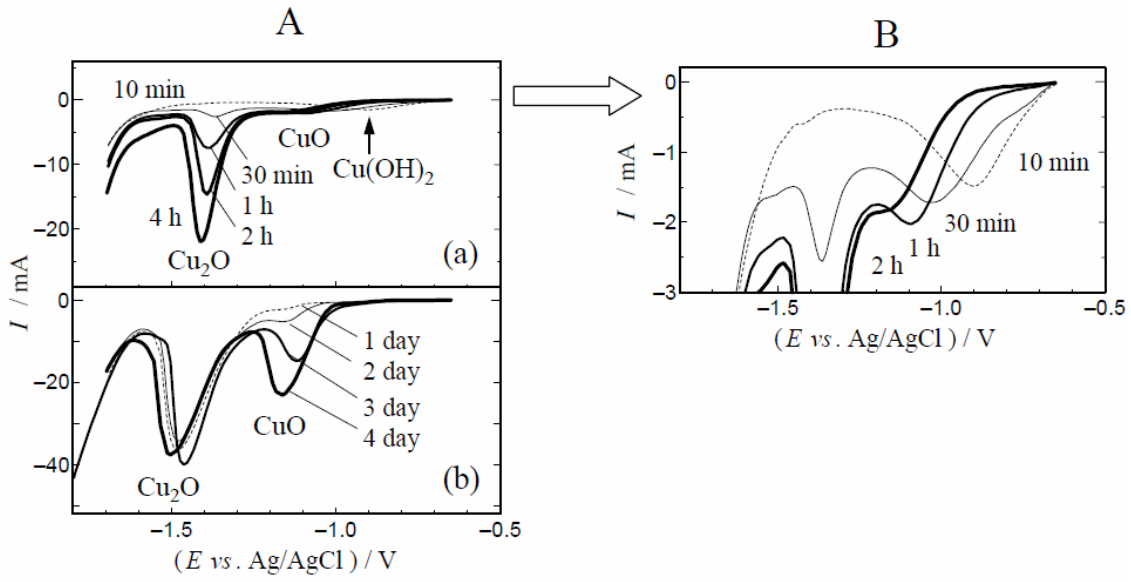

Figure 5.1 (A) Current–potential curves recorded by LSV for copper plates heated at 80 °C and RH 90% for (a) 10 min–4 h and for (b) 1 day–4 days. The current–potential curves in panel (a) are partially zoomed in Fig. 5.1B. Electrolyte solution: SAE. Scan rate: 100 mV s^{-1}.

Figure 5.2 shows the changes in the thicknesses of Cu_2O and CuO films with increase in the heating period at 80 °C and RH 90%. The small thickness (<2 nm) of the CuO film formed in the early stage of corrosion (<1 day) cannot be read from the plot in Fig. 5.2. However, the figure clearly shows that the initially formed thin film of CuO grew rapidly after the growth of the Cu_2O layer had stopped. Thus, there should be a certain threshold value of the Cu_2O layer thickness, *i.e.,* ~35 nm, above which the layer of CuO can grow extensively over the inner Cu_2O layer. A similar limiting thickness of a Cu_2O layer was previously observed for the growth of oxide films on copper single crystal surfaces in water.[12] Referring to the previous discussion, the limiting thickness of the Cu_2O layer might result from the competition of the proportionation reaction ($Cu + CuO \rightarrow Cu_2O$) and the CuO formation ($Cu_2O + (1/2)O_2 \rightarrow 2CuO$). The threshold value of the Cu_2O-layer thickness probably depends on unknown factors that govern the kinetics of the competing reactions. It should also be noted that after the threshold value was exceeded, an island-shaped structure of CuO films (grey color) was formed on the copper plate and spread over the whole plate by further heating.

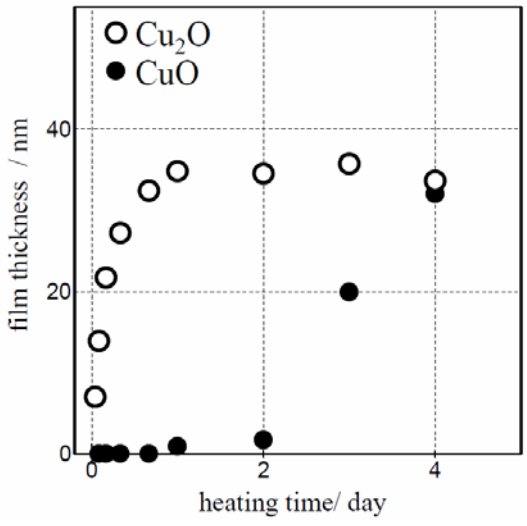

Figure 5.2 Changes in the thicknesses of Cu_2O and CuO films with increase in the heating period at 80 °C and RH 90%.

In order to understand the role of water in the corrosion processes, a corrosion test under dry conditions was carried out at 300 °C in a temperature-controlled oven. Figure 5.3 shows (A) current–potential curves and (B) powder XRD patterns (in θ-2θ scan) for copper plates heated at 300 °C for 10–30 min. The peaks of Cu_2O and CuO appeared and grew together. In the initial stage of corrosion, however, Cu_2O seems to have formed prior to CuO, since Cu_2O was the main oxide species formed by heating at a lower temperature, *i.e.*, 250 °C for 10 min (data not shown). The XRD patterns shown in Fig. 5.3B seems have broader diffraction peaks (see Fig. 5.5), suggesting that the grain size of the copper oxides formed at 300 °C was smaller. Probably due to this, the diffraction peaks for Cu_2O and CuO around 36 degrees were overlapped and could not be separately observed.

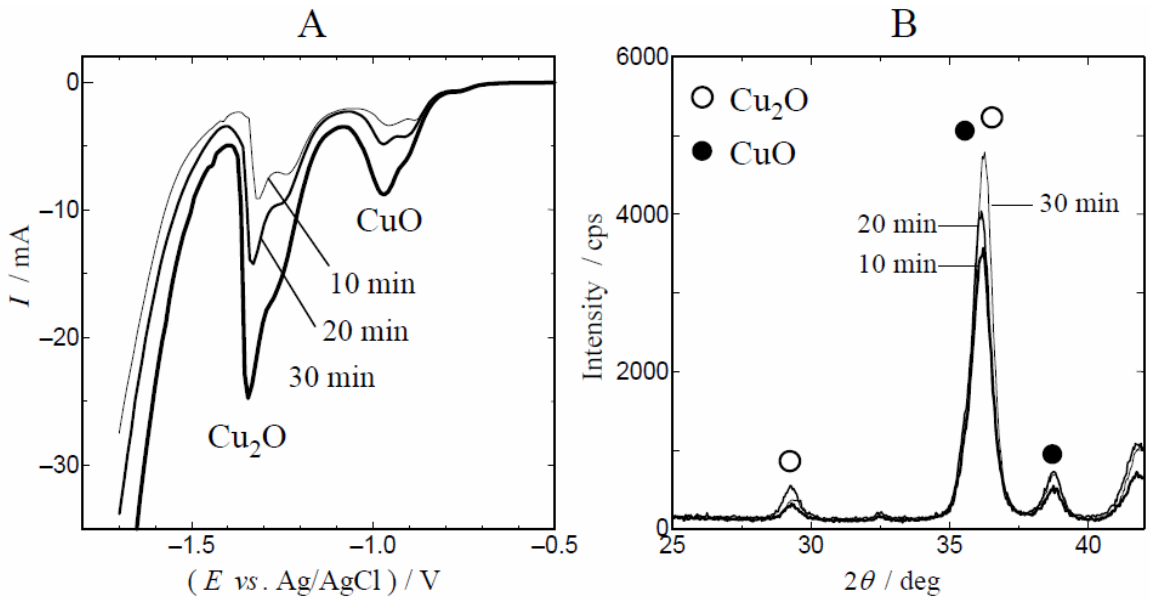

Figure 5.3 (A) Current–potential curves recorded by LSV with 6 M KOH + 1 M LiOH at 10 mV s^{-1} and (B) powder XRD patterns for copper plates heated at 300 °C for 10, 20, and 30 min.

In a previous paper on the corrosion of oxide-free copper plates at a higher temperature (350 °C),[13] it was reported that two layers of CuO and Cu_2O, the thicknesses of which were both about

300 nm, were formed within 25 min and that further heating up to 100 min made the oxide layers thicker (CuO: 600 nm, Cu_2O: 400 nm). This report is in harmony with our previous study,[13] in which the thicknesses of copper oxides formed at 300 °C for 20 min were estimated to be 200 nm for CuO and 400 nm for Cu_2O.

Thus, the corrosion behavior at higher temperatures such as 300 °C was relatively simple. The corrosion products were only CuO and Cu_2O. There was no formation of $Cu(OH)_2$ because of the absence of water.

5.3.2 Corrosion tests by immersion in alkaline solution

Figure 5.4 shows current–potential curves recorded in SAE for copper plates corroded by immersion in 1 M NaOH at 30 °C for (A) 1–30 min and (B) 8–32 h. For a short immersion period (*i.e.*, 1 min), both $Cu(OH)_2$ and CuO were formed and gradually grew until at least 30 min of immersion. Cu_2O was formed after a time lag of about 2 min and then grew with increase in the immersion period up to at least 8 h. However, the reduction peak of Cu_2O at around –1.4 V was almost constant in height for immersion periods of 8–32 h (Fig. 5.4B), indicating that the growth of Cu_2O stopped at 8 h after the start of immersion. After the growth of Cu_2O stopped, a CuO layer grew rapidly, as can be seen in the figure. After 16 h of immersion, the copper surface became black, suggesting the formation of a Cu/Cu_2O/CuO structure.[1,14] The corrosion behavior in 1 M NaOH was also confirmed by XRD measurements. Figure 5.5 shows powder XRD patterns (in θ-2θ scan) for copper plates immersed in 1 M NaOH at 30 °C for 8, 16, and 32 h. For all the immersion periods, diffraction patterns of Cu_2O were detected. Diffraction patterns of CuO were detected for immersion periods over 16 h. This observation is in harmony with the voltammetric behaviors shown in Fig. 5.4B.

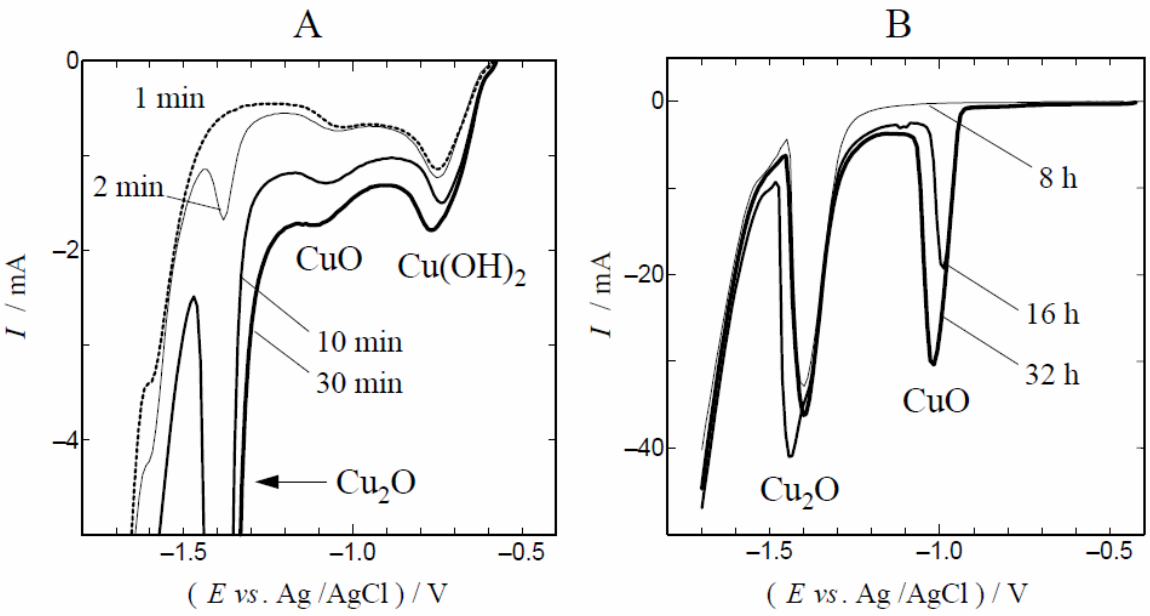

Figure 5.4 Current–potential curves recorded by LSV with 6 M KOH + 1 M LiOH for copper plates immersed in 1 M NaOH at 30 °C for (A) 1–30 min and (B) 8–32 h. Scan rate: (A) 100 mV s^{-1} and (B) 10 mV s^{-1}.

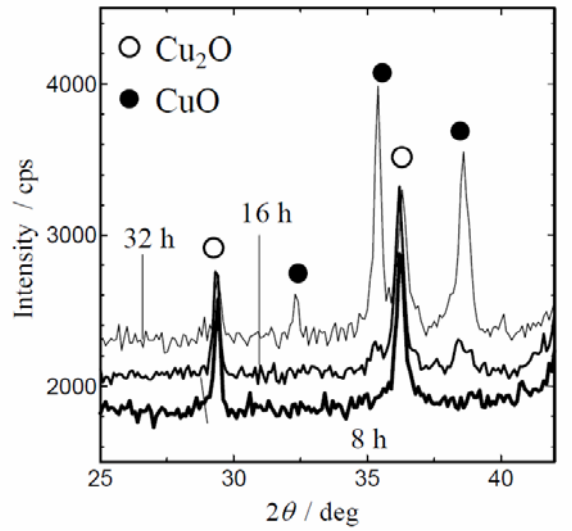

Figure 5.5 Powder XRD patterns for copper plates immersed in 1 M NaOH at 30 °C for 8–32 h.

5.3.3 Growth mechanism of copper oxides

Based on the above experimental results, the corrosion mechanism of copper in the

atmosphere will be discussed below.

Under the experimental conditions in the presence of water, the copper surface is first oxidized by oxygen to form $Cu(OH)_2$ on the surface:

$$Cu + (1/2)O_2 + H_2O \rightarrow Cu(OH)_2 \quad (5.1)$$

See also Fig. 5.6, which shows a proposed mechanism for the atmospheric corrosion of copper.

Thus, $Cu(OH)_2$ is first formed on an uncorroded surface in the initial stage of the atmospheric corrosion. When the corrosion is advanced, however, $Cu(OH)_2$ is converted by dehydration to CuO according to the reaction:

$$Cu(OH)_2 \rightarrow CuO + H_2O \quad (5.2)$$

The thus-formed CuO layer, however, is of several molecules in thickness (about 2 nm) and does not grow with further progression of corrosion. This is due to the proportionation reaction between the base metal copper and the thin CuO layer:

$$CuO + Cu \rightarrow Cu_2O \quad (5.3)$$

Once Cu_2O is formed, the inner oxide layer grew selectively. However, the growth of the inner Cu_2O layer appears to stop after a certain time lag under given conditions. Instead, the surface CuO layer grows again rapidly.

$$Cu_2O + (1/2)O_2 \rightarrow 2CuO \quad (5.4)$$

Unlike the CuO layer formed in the earlier stage of corrosion, the CuO layer in the late stage

can grow rapidly after the thickness of the Cu_2O layer reaches a certain level.[1,2] In contrast to the rapid growth of the outer CuO layer, the growth of the inner Cu_2O layer is limited, probably because of the competition of the proportionation reaction (Eq. 5.3) and the CuO formation (Eq. 5.4).[12] The proportionation reaction is unfavorable for a thicker Cu_2O layer because the electron-transport distance between metal Cu and CuO is longer for a thicker film. Accordingly, the formation of CuO may occur preferentially after the thickness of the Cu_2O layer reaches a threshold value.

The present study thus showed that typical corrosion of copper in the atmosphere proceeded as in Fig. 5.5. However, the exposure conditions chosen in our study are just representative. The universality of the proposed mechanism should be examined by further corrosion tests under various exposure conditions.

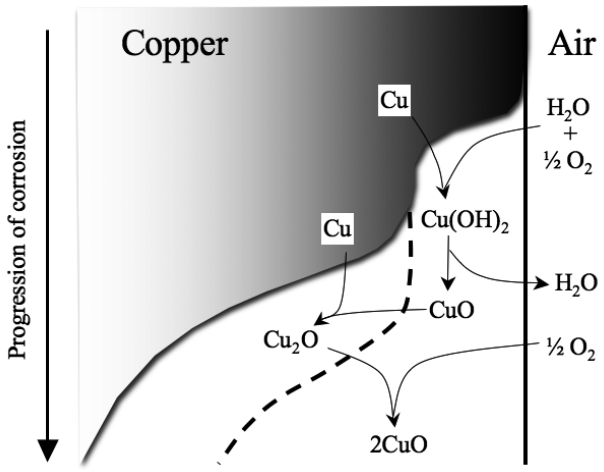

Figure 5.6 Proposed mechanism for the atmospheric corrosion of copper.

References

1. S. Nakayama, A. Kimura, M. Shibata, S. Kuwabata, and T. Osakai, *J. Electrochem. Soc.*, **148**, B467 (2001).
2. S. Nakayama, M. Shibata, S. Kuwabata, T. Osakai, and T. Notoya, *Zairyo-to-Kankyo*, **51**, 566 (2002), in Japanese; the English translation is available in *Corros. Eng.*, **51**, 787 (2002).
3. R. L. Deutscher and R. Woods, *J. Appl. Electrochem.*, **16**, 413 (1986).
4. M. Lenglet, K. Kartouni and D. Delahaye, *J. Appl. Electrochem.*, **21**, 697 (1991).
5. M. Lenglet, J. Lopitaux, C. Leygraf, I. Odnevall, M. Carballeira, J. C. Noualhaguet, J. Guinement, J. Gautier, and J. Boissel, *J. Electrochem. Soc.*, **142**, 3690 (1995).
6. D.L. Cocke, R. Schennach, M. A. Hossain, D. E. Mencer, H. McWhinney, J. R. Parga, M. Kesmez, J.A.G. Gomes, and M.Y.A. Mollah, *Vacuum*, **79**, 71 (2005).
7. J.M. Bastidas, A. Lopez-Delgado, E. Cano, J. L. Polo, and F. A. Lopez, *J. Electrochem. Soc.*, **147**, 999 (2000).
8. J.M. Smith, J. C. Wren, M. Odziemkowski, and D. W. Shoesmith, *J. Electrochem. Soc.*, **154**, C431 (2007).
9. S.M. Abd El Haleem and E. E. Abd El Aal, *Corrosion*, **62**, 121 (2006).
10. J. Gomez Becerra, R. C. Salvarezza, and A. J. Arvia, *Electrochim. Acta*, **33**, 613 (1988).
11. S. Nakayama, T. Notoya, and T. Osakai, *J. Electrochem. Soc.*, **157**, C289 (2010).
12. J. Kruger, *J. Electrochem. Soc.*, **108**, 503 (1961).
13. M. Honkanen, M. Vippola, and T. Lepistö, *J. Mater. Res.*, **23**, 1350 (2008).
14. S. Nakayama, T. Kaji, T. Notoya, and T. Osakai, *J. Electrochem. Soc.*, **154**, C1 (2007).

Chapter 6. Application to Tin

6.1 Introduction

Tin is widely used in industrial processes for plating and alloying. Although tin is relatively corrosion-resistant, its oxide layers comprising SnO (black) and SnO_2 (white) phases of various thicknesses are formed on surfaces that are exposed to air, usually containing moisture and pollutants. Then, various problems such as tarnishing, soldering defects, and tin-whiskers occur depending on the thickness and kind of the oxide. For example, SnO_2 has been reported to degrade solder wettability more extensively than SnO.[1] However, tin oxides have not been determined quantitatively by means of existing analytical methods.

In addition to oxides, hydroxides such as $Sn(OH)_2$ and $Sn(OH)_4$ may form on tin surfaces. In the following remarks, however, $Sn(OH)_4$ will be described as hydrated stannous oxide "$SnO_2 \cdot nH_2O$" according to the conventional way. Since tin hydroxides are less stable than the corresponding oxides, they may gradually change to oxides.[2]

Surface analytical techniques such as XPS,[3,4] XRD,[5] and surface-enhanced Raman scattering (SERS)[6] have been employed for characterization of tin compounds on surfaces. These spectrophotometric techniques are useful for qualitative analyses but not always adequate for quantitative analyses. It has also been reported that separation of SnO and SnO_2 is difficult by XPS.[7]

CP is an electrochemical technique that has frequently been applied to quantitative analysis of oxide films formed on tin surfaces. In this technique, oxide films are electrochemically reduced by flowing at a constant current through a tin sample, and the resulting change in electrode potential for the tin sample is recorded as a function of time. The amount of tin oxides can be determined from the quantities of electricity required for reduction of the oxides. However, there has been no report on estimation of the amounts of tin hydroxides by CP.

Reduction of tin oxides in various electrolyte solutions, such as 0.01 M KCl,[8] 0.1 M KCl,[9]

dilute HCl,[10] dilute HBr,[9,10] and 0.1 M Na_2CO_3,[11] has been performed for electrochemical characterization of oxidized tin samples. However, the quantitative values were dependent on the electrolytes used.[9,10] In recent years, borate buffer solution[1,4] (0.1 M H_3BO_3 + 0.025 M $Na_2B_4O_7$) has been frequently used as a supporting electrolyte because there is almost no reaction of this electrolyte with tin oxides. It should be noted that the magnitude of current density used in CP measurements, as well as the kind and concentration of electrolytes, has an effect on quantitative values for tin oxides.[1,4,10] Thus, CP has not yet been established as a standard method for the characterization of tin oxide films.

Electrochemical analysis of copper oxides has a longer history than for that of tin oxides. However, until recently, there has been no report on the optimization of experimental conditions for the determination of copper oxides by CP or other electrochemical methods such as voltammetry. As described in the above chapters, we have recently shown that the use of a strongly alkaline electrolyte (6 M KOH + 1 M LiOH) enabled selective and reliable determination of copper oxides.[12,13] Based on this experience, we carried out the present study and found that an ammonia buffer solution (0.5 M NH_4OH + 0.5 M NH_4Cl) was suitable for selective determination of tin oxides (or hydroxides) by LSV.

6.2. Experimental

6.2.1. Samples

Anhydrous SnO and SnO_2 were supplied by Wako Pure Chemicals Ltd., Osaka. $SnO_2 \cdot nH_2O$ (>84.1% as SnO_2) was supplied by Mitsuwa Chemicals Ltd., Osaka. In addition to these standard powder samples, a chemically produced tin oxide powder sample was prepared by heating at 180 °C for 2 h a precipitate that was formed by titration of a solution of $SnCl_4$ (obtained from Wako Pure Chemicals Ltd.) with a NaOH solution.[6] Each powder sample was mixed with a carbon paste consisting of graphite powder and paraffin oil (both available from ALS Co., Ltd., Tokyo), with the weight ratio of the sample and the carbon paste being 1:5. The resulting mixture (*ca*. 0.5 mg)

was spread over a glassy carbon disc electrode (3 mm-ϕ) to prepare a carbon paste electrode.[14] A glassy carbon electrode for special use was also purchased from ALS Co., Ltd.

In addition to the powder samples, tin plates (0.5 mm in thickness; The Nilaco Corporation SN-443461; 99.9% purity) were used for corrosion tests in the atmosphere. A tin plate was cut into 5 mm × 50 mm pieces and then etched in 6 M hydrochloric acid, followed by rinsing successively with distilled water and ethanol. Oxide films were then prepared on the tin plate by heating in a temperature/humidity-controlled chamber at 80 °C and RH 90% and by heating in a temperature-controlled chamber at 180 °C or 200 °C. One end of the treated tin plate (geometric area = 1.0 cm^2) served as the working electrode, with the other area being masked with a PTFE seal tape.

6.2.2. Electrochemical measurements

LSV measurements were carried out in the same manner as shown in § 2.2.2. A potential sweep was performed from a rest potential to the potential for hydrogen evolution at the rate of 2, 5, and 10 mV s^{-1}.

The electrolyte solutions used were 0.1–2 M NH_4OH + NH_4Cl (pH 9.1–9.5) and 0.1 M H_3BO_3 + 0.025 M $Na_2B_4O_7$ (pH 8.4), all of which were not deaerated. All of the reagents used for preparation of the electrolyte solutions were of analytical grade (Wako Pure Chemicals Ltd.).

6.2.3. XRD measurements

A Philips X'Pert-Pro XRD system using Cu Kα radiation (45 kV, 40 mA) was used to characterize the powder samples by measuring powder XRD patterns (in θ-2θ scan). Oxide films on tin plates were also analyzed by the same apparatus with a grazing incident angle of 1 degree. In the geometry, crystalline thin films with a thickness of less than 100 nm are detectable.

6.3. Results and Discussion

6.3.1. Search for suitable electrolyte

CP and LSV have been frequently applied for determination of corrosion products formed on metals including copper, silver, and tin. Both techniques should provide equivalent information on corrosion products if the optimum measurement conditions can be established. However, since LSV gives peak-like signals that are easy to analyze, we have employed this technique to study corrosion products formed on tin surfaces.

Panel (a) of Fig. 6.1 shows current–potential curves recorded by LSV for three powder samples (anhydrous SnO and SnO_2 and hydrated SnO_2 denoted as "$SnO_2{\cdot}nH_2O$") in a borate buffer solution (0.1 M H_3BO_3 + 0.025 M $Na_2B_4O_7$). This buffer solution is frequently used as a supporting electrolyte for electrochemical determination of tin oxides. The small current peak appearing around –0.6 V is ascribed to the base material of the carbon paste electrode. As shown in panel (a) of Fig. 6.1, all of the oxide samples gave a reduction peak (for SnO and $SnO_2{\cdot}nH_2O$) or increased the cathodic final descent (for SnO_2). It was thus shown that these tin oxides were definitely reduced in the borate buffer. However, the reduction peaks for SnO and $SnO_2{\cdot}nH_2O$ were very broad, suggesting lower reduction rates in the buffer solution. It was also found that the peak area of $SnO_2{\cdot}nH_2O$ was much smaller than that of SnO. This suggests that the reduction efficiency for $SnO_2{\cdot}nH_2O$ was considerably low in the borate buffer solution for an unknown reason. Regarding the potential where the reduction current started to flow, the potential for SnO was more positive than that for $SnO_2{\cdot}nH_2O$. This is reasonable, since SnO has a higher reduction potential than that of SnO_2 at around pH 8.4 (for the borate buffer).[1,4] However, it should be noted that the reduction peak potentials of these two oxides were almost the same, indicating that selective determination of the oxides is difficult under such measurement conditions. These results suggested that previous studies using the borate buffer were conducted in an inappropriate manner.

We then searched for an electrolyte that is suitable for the present purpose, giving two separate current peaks for the reduction of SnO and SnO_2 (or $SnO_2{\cdot}nH_2O$). As a result of trial and error, we found that an electrolyte containing NH_4^+ ions is suitable for the selective determination

of the tin oxides.

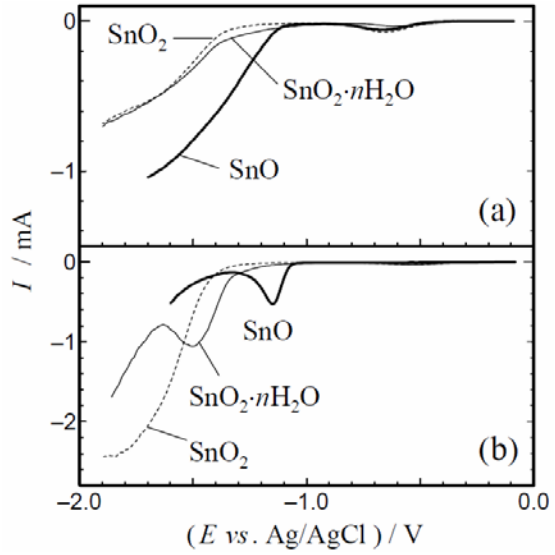

Figure 6.1 Current–potential curves recorded by LSV for powder samples of SnO, SnO_2, and $SnO_2{\cdot}nH_2O$. Electrolyte solutions: (a) 0.1 M H_3BO_3 + 0.025 M $Na_2B_4O_7$ and (b) 0.5 M NH_4OH + 0.5 M NH_4Cl. Scan rate: 10 mV s^{-1}.

Panel (b) of Fig. 6.1 shows current–potential curves recorded by LSV for the three powder samples in an ammonia buffer (0.5 M NH_4OH + 0.5 M NH_4Cl). This buffer composition was found to be the most suitable for this purpose, as described below. It should be stressed here that we could obtain two well-defined peaks for the reduction of SnO and $SnO_2{\cdot}nH_2O$ by using this electrolyte. These peaks were well separated by ~0.3 V. The peak area of $SnO_2{\cdot}nH_2O$ was relatively large compared with that observed in the borate buffer (panel (a) of Fig. 6.1). The reduction efficiency thus appeared to be higher in the ammonia buffer. It should also be noted that SnO and $SnO_2{\cdot}nH_2O$ were reduced under these conditions in accordance with the thermodynamic order.[1,4] As also shown in panel (b) of Fig. 6.1, a reduction peak was also observed for anhydrous SnO_2, though the peak potential was lower than that of the hydrated form "$SnO_2{\cdot}nH_2O$". This seems to be due to the difference in crystal size between anhydrous and hydrated SnO_2's, as discussed below.

Since a single reduction peak was observed for each oxide, the reduction of tin oxides seemed to occur in one step as

$$SnO + H_2O + 2e^- \rightarrow Sn + 2OH^- \quad (6.1)$$

$$SnO_2 \cdot nH_2O + 2H_2O + 4e^- \rightarrow Sn + nH_2O + 4OH^- \quad (6.2)$$

$$SnO_2 + 2H_2O + 4e^- \rightarrow Sn + 4OH^- \quad (6.3)$$

Figure 6.2 shows the powder XRD patterns for three tetravalent tin oxides, *i.e.*, anhydrous SnO_2, hydrated $SnO_2 \cdot nH_2O$, and chemically prepared SnO_2. The last powder sample was prepared by thermally dehydrating a precipitate of tin hydroxide formed by titration, as described above. Since this preparation process is similar to the corrosion process in the atmosphere, the chemically prepared SnO_2 sample would be useful for the simulated corrosion product. As can be seen in Fig. 6.2, the anhydrous SnO_2 gave rise to sharp diffraction patterns. On the other hand, the $SnO_2 \cdot nH_2O$ sample and the chemically prepared SnO_2 showed broad diffraction patterns. The diffraction angles were almost the same in the three powder samples, indicating that all of the SnO_2 powder samples had a common crystalline structure. However, the crystal sizes estimated by Scherrer's equation[15] from the broadening of the diffraction patterns were about 23 nm for the anhydrous SnO_2 and about 3 nm for both the $SnO_2 \cdot nH_2O$ sample and the chemically prepared SnO_2. Probably because of the large crystal size, the reduction of anhydrous SnO_2 seemed to be kinetically difficult to occur even in the ammonia buffer (see again Fig. 6.1(b)).

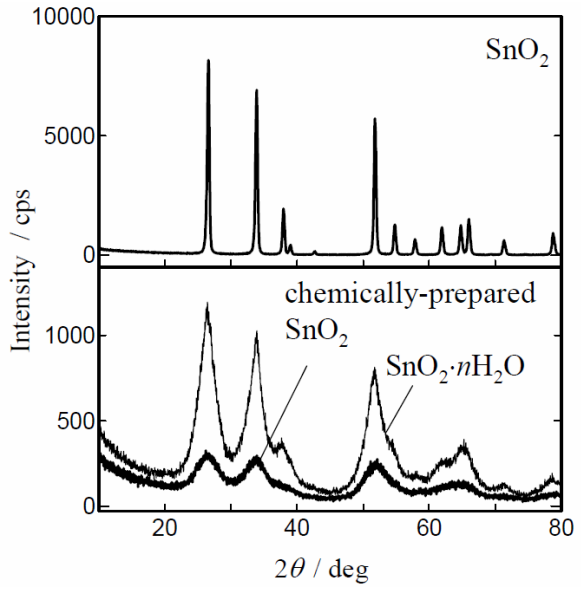

Figure 6.2 XRD patterns for powder samples of SnO_2, $SnO_2{\cdot}nH_2O$, and the chemically prepared SnO_2.

Though the data are not shown, the chemically prepared SnO_2 showed a current–potential curve similar to that of the $SnO_2{\cdot}nH_2O$ sample. Taking into account the similarity of the powder XRD patterns (Fig. 6.2), we concluded that the chemically prepared SnO_2 was identical to the $SnO_2{\cdot}nH_2O$ sample in chemical and crystalline structures. It was thus thought that the tetravalent tin oxide formed on tin surfaces in air is $SnO_2{\cdot}nH_2O$.

6.3.2. Preparation of a standard sample containing SnO and $SnO_2{\cdot}nH_2O$

Based on the above fundamental results, we tried to prepare a standard tin plate sample containing both SnO and $SnO_2{\cdot}nH_2O$ in comparable amounts, in view of optimization of the analytical conditions.

As the formation of oxides on metal surfaces is generally affected by temperature and relative humidity (RH), we corroded tin plates by heating under various temperature and humidity conditions. It was observed that the color of the tin surface became black with heating at a

temperature above 100 °C and became white with heating at a temperature below 100 °C with high RH. Figure 6.3 shows current–potential curves recorded by LSV with 0.5 M NH_4OH + 0.5 M NH_4Cl for tin plates heated for various periods (4–32 h) at 180 °C and at 80 °C with RH of 90%. As can be seen in Fig. 6.3, two distinct peaks appeared at different potentials (–1.15 V and –1.4 V). Referring to the results in panel (b) of Fig. 6.1, it was found that anhydrous SnO was formed selectively at 180 °C (*i.e.*, with no humidity) and that hydrated $SnO_2 \cdot nH_2O$ was only formed at a lower temperature (80 °C) but with a higher RH (90%).

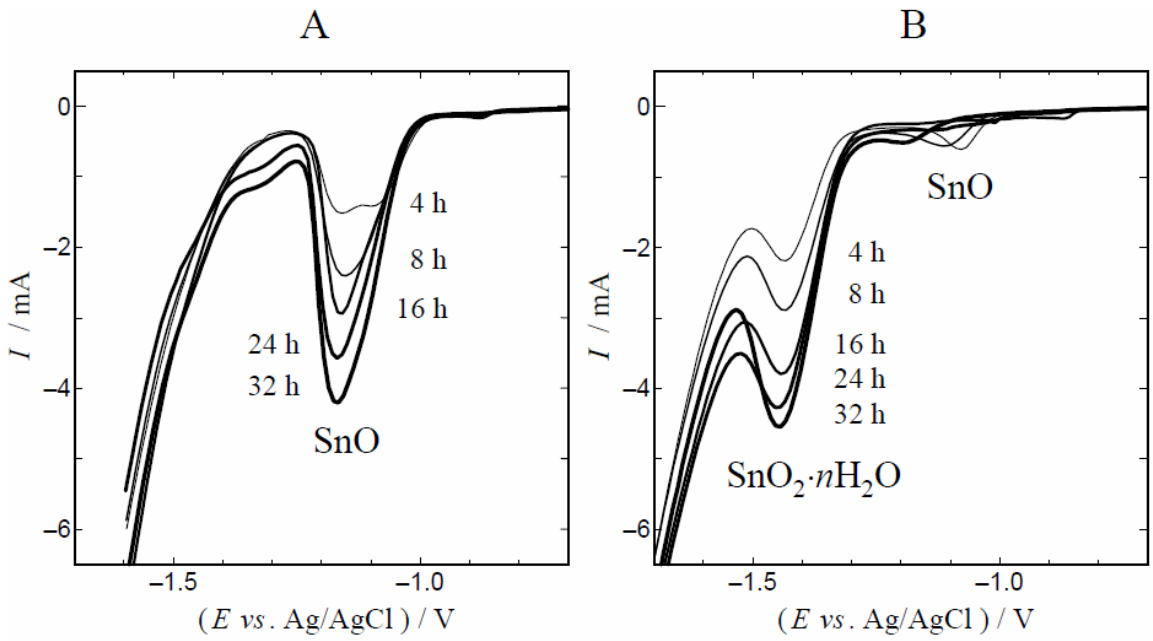

Figure 6.3 Current–potential curves recorded by LSV with 0.5 M NH_4OH + 0.5 M NH_4Cl for tin plates heated (a) at 180 °C and (b) at 80 °C–RH 90% for 4–32 h. Scan rate: 10 mV s^{-1}.

The average thickness of the SnO film (theoretical density = 6.44) formed at 180 °C for 32 h was estimated to be about 0.051 μm from the peak area. Although the theoretical density is unknown for $SnO_2 \cdot nH_2O$, the average thickness of the oxide film formed at 80 °C–RH 90% for 32 h was estimated to be about 0.06 μm, by assuming that the theoretical density of $SnO_2 \cdot nH_2O$ is the same as that of SnO.

On the basis of these findings, we prepared two different oxides on tin plates by heating at 180 °C for 6 h and successively heating at 80 °C–RH 90% for various periods (4–24 h). The current–potential curves observed for the plate samples in 0.5 M NH_4OH + 0.5 M NH_4Cl are shown in Fig. 6.4. The peak for $SnO_2{\cdot}nH_2O$ was increased by increasing the heating time at 80 °C–RH 90%. Since comparable peak areas for SnO and $SnO_2{\cdot}nH_2O$ were obtained by heating for 24 h, the sample prepared under these conditions was used for the "standard tin plate sample". From the above findings, it is apparent that SnO is firstly reduced, followed by the reduction of $SnO_2{\cdot}nH_2O$.

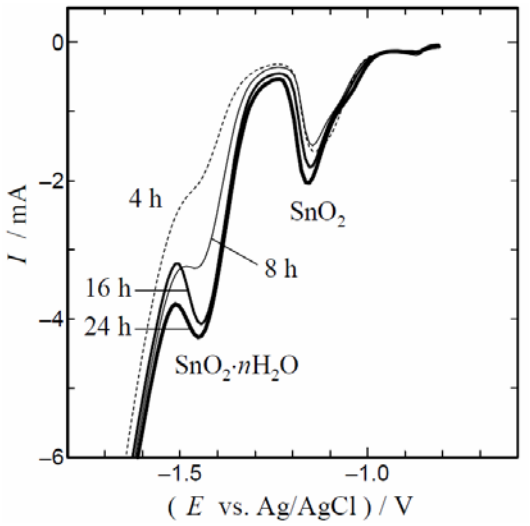

Figure 6.4 Current–potential curves recorded by LSV with 0.5 M NH_4OH + 0.5 M NH_4Cl for tin plates heated at 180 °C for 4 h and successively at 80 °C–RH 90% for various periods (4–24 h). Scan rate: 10 mV s^{-1}.

6.3.3. Effects of the concentration and composition of ammonia buffer

Using the thus prepared "standard tin plate sample", we optimized the concentration and the composition of the ammonia buffer for the simultaneous determination of SnO and $SnO_2{\cdot}nH_2O$.

Figure 6.5 shows current–potential curves for the "standard tin plate sample" that were recorded by LSV using various concentrations of ammonia buffer solutions with equal

concentrations of NH_4OH and NH_4Cl. When the buffer concentration was lower than 0.3 M, the reduction peak of $SnO_2{\cdot}nH_2O$ was not clear, possibly because of the lowering of the reduction efficiency. Although the peak became sharper with increase in the buffer concentration, the cathodic final descent due to hydrogen evolution became larger, making more difficult the determination of the peak current for the reduction of $SnO_2{\cdot}nH_2O$.

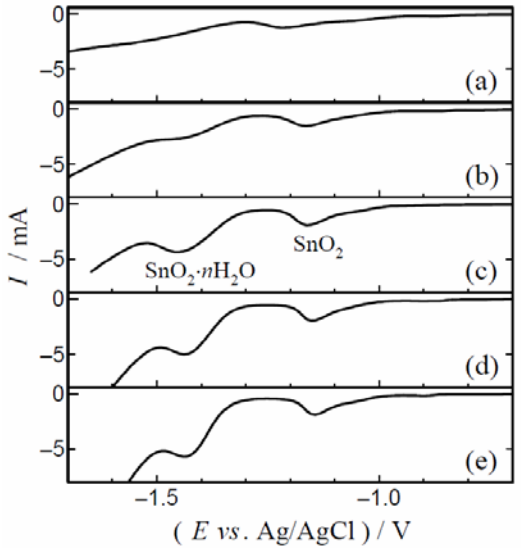

Figure 6.5 Current–potential curves for the "standard tin plate sample" (prepared by heating at 180 °C for 4 h and successively at 80 °C–RH 90% for 24 h) that were recorded by LSV with various concentrations of ammonia buffer (x M NH_4OH + x M NH_4Cl). x = (a) 0.1 M, (b) 0.3 M, (c) 0.5 M, (d) 1.0 M, and (e) 2.0 M. Scan rate: 10 mV s^{-1}.

Figure 6.6 shows current–potential curves for the "standard tin plate sample" that were recorded by LSV using ammonia buffers with different ratios of NH_4OH and NH_4Cl concentrations (the total concentration, *i.e.*, [NH_4OH] + [NH_4Cl], being set to 1 M). When [NH_4OH] was 1 M and [NH_4Cl] was 0 M, no clear reduction peaks were observed. With decrease in the [NH_4OH]/[NH_4Cl] ratio (*i.e.*, with lowering of pH), the reduction peak of $SnO_2{\cdot}nH_2O$ became sharper, but the cathodic final descent for hydrogen evolution became more significant.

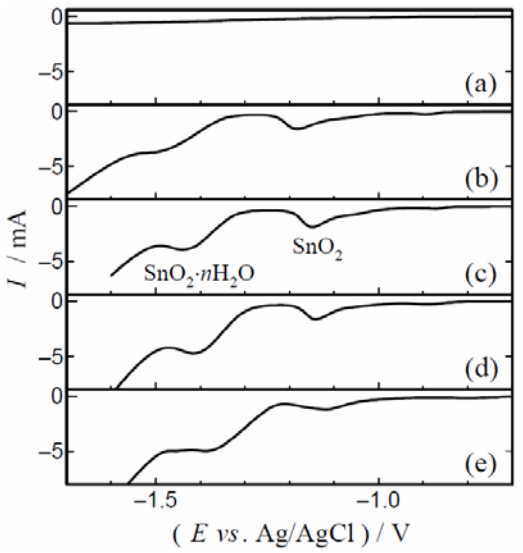

Figure 6.6 Current–potential curves for the "standard tin plate sample" that were recorded by LSV with ammonia buffer solutions having different $[NH_4OH]/[NH_4Cl]$ ratios: (a) 1/0 (pH 11.6), (b) 0.75/0.25 (pH 9.8), (c) 0.5/0.5 (pH 9.3), (d) 0.25/0.75 (pH 8.8), and (e) 0/1 (pH 5.25) (with $[NH_4OH] + [NH_4Cl] = 1$ M). Scan rate: 10 mV s^{-1}.

Considering the results shown in Figs. 6.5 and 6.6, we chose the 0.5 M NH_4OH + 0.5 M NH_4Cl buffer as a suitable electrolyte for selective determination of tin oxides.

In Fig. 6.7, the current–potential curve for the "standard tin plate sample" in the borate buffer solution is compared with that for the "standard tin plate sample" in the ammonia buffer solution (0.5 M NH_4OH + 0.5 M NH_4Cl). Two well-defined peaks for the reduction of SnO and $SnO_2 \cdot nH_2O$ were observed using the ammonia buffer, whereas only one distinct peak (for SnO?) was detected using the borate buffer. These results are in line with the results for the powder samples shown in Fig. 6.1. Although data not shown, when 1 M KCl or 1 M Na_2CO_3 was used for the supporting electrolyte, we obtained a reduction peak for SnO, but no distinct peak for $SnO_2 \cdot nH_2O$.

As described above, the ammonia buffer has a significant facilitation effect particularly on the electrochemical reduction of $SnO_2 \cdot nH_2O$. The origin of this effect is not clear at this stage, but may

be related to the characteristics of SnO_2 as an n-type semiconductor. So far, SnO_2 has been used as the sensing material of ammonia gas sensors.[16-18] On the surface of SnO_2, O_2 molecules are absorbed, and they extract electrons from the conduction band of SnO_2. This leads to a band bending and an electron-depleted region, the so-called space-charge region, which results in the lowering of conductivity. Reaction of the absorbed oxygen species with reducing gases such as ammonia can reverse the band bending, thereby increasing the conductivity. It seems reasonable to imagine that a similar situation may arise in the electrochemical reaction of $SnO_2 \cdot nH_2O$ in solutions containing NH_4^+ ions. Supposing O_2 molecules are absorbed on a tin plate sample prepared in air, they may decrease the conductivity of $SnO_2 \cdot nH_2O$ layer, thus lowering the reduction efficiency. When NH_4^+ ions are present in the electrolyte solution, they can access easily to the negatively charged surface of the tin electrode and therein react with the absorbed O_2 molecules. Possibly, this may enhance the reduction efficiency for $SnO_2 \cdot nH_2O$. For the use of the borate buffer, KCl, and Na_2CO_3, the electrolyte cations (*i. e.*, Na^+ and K^+) cannot react with the absorbed O_2 molecules, and thus there would be no facilitation effect for the reduction of $SnO_2 \cdot nH_2O$.

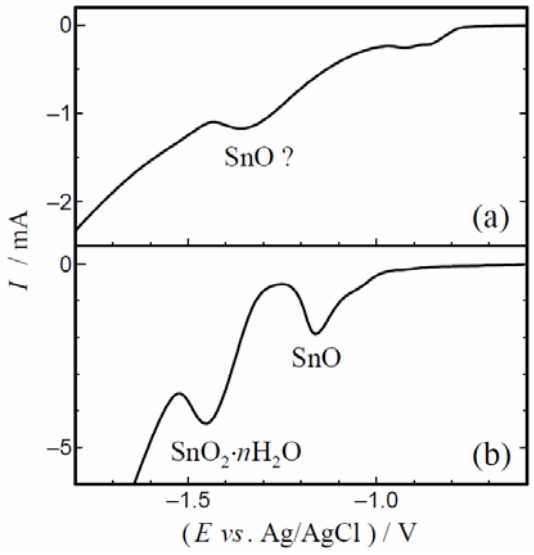

Figure 6.7 Current–potential curves for the "standard tin plate sample" that were recorded by LSV with (a) 0.1 M H_3BO_3 + 0.025 M $Na_2B_4O_7$ and with (b) 0.5 M NH_4OH + 0.5 M NH_4Cl. Scan rate: 10 mV s^{-1}.

6.3.4. Identification of reduction peaks by thin-layer XRD

The above-described results suggested that the main oxide species formed on tin by atmospheric corrosion are SnO and $SnO_2 \cdot nH_2O$. In order to verify this, we employed thin-layer XRD for direct identification of the reduction peaks of tin oxides. For ensuring the peak assignment, tin plates were corroded in stronger corrosive environments: 200 °C for 10 days (for sample (a)) and 30 °C for 6 days (for sample (b)) in 0.01 M NaOH. The current–potential curves recorded by LSV and the XRD patterns are shown in Fig. 6.8(A) and 6.8(B), respectively. From the LSV and XRD data for sample (a), we concluded that the peak at a higher potential is due to the reduction of SnO. On the other hand, the diffraction peaks of SnO_2, though weak, were observed for sample (b), while there were no peaks of SnO. The half width of the weak peaks is similar to that for $SnO_2 \cdot nH_2O$ or the chemically prepared SnO_2 shown in Fig. 6.2. Accordingly, the reduction peak appearing at a lower potential was concluded to be due to the reduction of $SnO_2 \cdot nH_2O$.

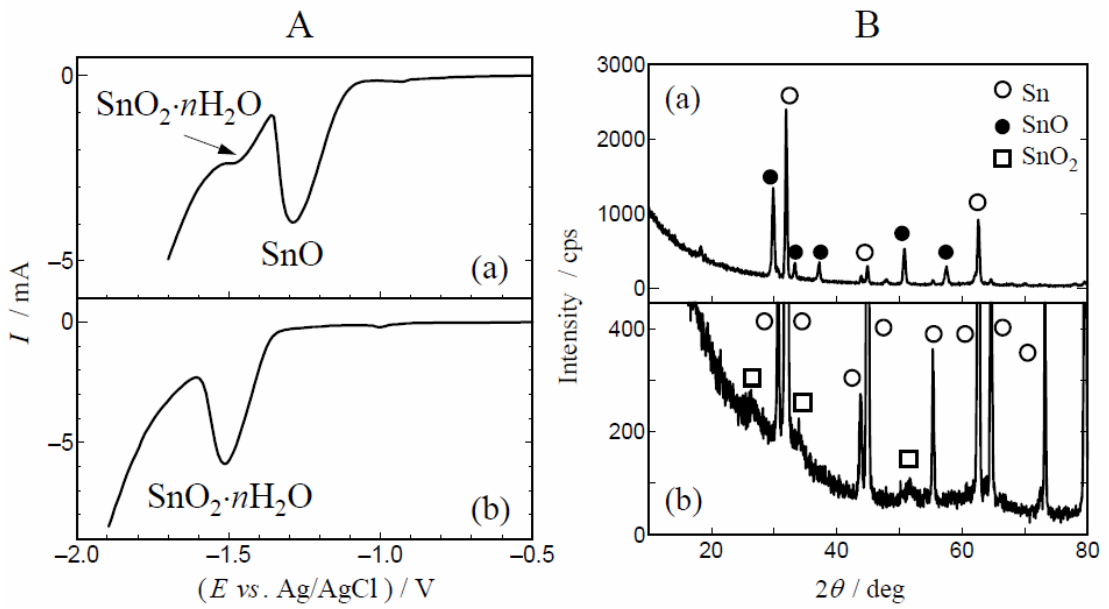

Figure 6.8 (A) Current–potential curves recorded by LSV with the 0.5 M NH_4OH + 0.5 M NH_4Cl buffer and (B) XRD patterns obtained by the grazing incident method for tin plates heated (a) at 200 °C for 10 days and (b) at 30 °C for 6 days in 0.01 M NaOH. Scan rate: (a) 5 mV s^{-1} and (b) 2 mV s^{-1}.

References

1. D. Morgan Tench, D. P. Anderson, and P. Kim, *J. Appl. Electrochem.*, **24**, 18 (1994).
2. C. I. House and G. H. Kelsall, *Electrochim. Acta* **29**, 1459 (1984).
3. M. Seruga, M. Metikos-Hukovic, T. Valla, M. Milun, H. Hoffschultz, and K. Wandelt, *J. Electroanal. Chem.*, **407**, 83 (1996).
4. S. Cho, J. Yu, S. K. Kang, and D.-Y. Shih, *J. Electron. Mater.*, **34**, 635 (2005).
5. M. Nagasaka, H. Fuse, and T. Yamashina, *Thin Solid Films*, **29**, L29 (1975).
6. B. X. Huang, P. Tornatore, and Y.-S. Li, *Electrochim. Acta*, **46**, 671 (2000).
7. Z. Liu, K. Handa, K. Kaibuchi, Y. Tanaka, and J. Kawai, *J. Electron Spectrosc. Relat. Phenom.*, **135**, 155 (2004).
8. F. W. Salt and J. G. N. Thomas, *Nature*, **178**, 434 (1956).
9. A. R. Willey and D. F. Kelsey, *Anal. Chem.*, **30**, 1804 (1958).
10. R. P. Frankenthal, T. J. Butler, and R. T. Davis, Jr., *Anal. Chem.*, **30**, 441 (1958).
11. S. Wolynec and D. R. Gabe, *Brit. Corros. J.*, **6**, 271 (1971).
12. S. Nakayama, A. Kimura, M. Shibata, S. Kuwabata, and T. Osakai, *J. Electrochem. Soc.*, **148**, B467 (2001).
13. S. Nakayama, T. Notoya, and T. Osakai, *J. Electrochem. Soc.*, **157**, C289 (2010).
14. S. Nakayama, M. Shibata, T. Osakai, and T. Notoya, *Journal of the JRICu,* **43**, 235 (2004).
15. P. Scherrer, *Nachr. Ges. Wiss. Göttingen*, **26**, 98 (1918).
16. A. Teeramongkonrasmee and M. Sriyudthsak, *Sens. Actuators* B, **106**, 256 (2000).
17. K.K. Khun, A. Mahajan and R.K.Bedi, *J. Appl. Phys.*, **106**, 124509 (2009).
18. C. Wang, L. Yin, L. Zhang, D.Xiang and R. Gao, *Sensors*, **10**, 2088 (2010).

Summary

In this thesis the author has developed a new voltammetric method using a strongly alkaline electrolyte (SAE) for the quantitative characterization of copper corrosion products.

In chapter 1, the history of the analysis of copper corrosion products is reviewed and the objective of this research is presented. For the determination of copper oxides (*i.e.*, Cu_2O and CuO) and sulfide (Cu_2S), electrochemical techniques including chronopotentiometry (CP) and linear sweep voltammetry (LSV) have been applied since more than 70 years. In these conventional methods, a neutral or weak alkaline electrolyte such as 0.1 M KCl is used, and there have been serious problems: (1) a worse separation between the reduction potentials of Cu_2O and CuO and (2) an ambiguity of the reduction order of the copper oxides.

In chapter 2, the outline of the developed voltammetric method is described. In order to solve the above first problem (1), I focused on the optimization of supporting electrolyte for achieving enough separation between the reduction peaks of Cu_2O and CuO. By a detailed investigation, it was found that the reduction potential of CuO was hardly affected by the kind of electrolytes; however the reduction of Cu_2O was strongly suppressed by (a) the presence of Li^+ ions and (b) high alkalinity. It was then shown that a SAE composed of 6 M KOH + 1 M LiOH was very suitable for highly selective determination of the copper oxides. The high quantitative capability of the established method for the determination of Cu_2O and CuO has also been demonstrated.

The second serious problem (2) in the conventional methods is dealt in chapter 3. For a long time, there have been conflicting views regarding the reduction order of Cu_2O and CuO. To determine the order, we prepared a standard sample of CuO/Cu_2O/Cu, which was partially reduced by constant-current electrolysis (*i.e.*, in a CP mode), and then the residual oxide species were identified by LSV with SAE and X-ray diffraction (XRD). It was revealed that CuO was firstly reduced, followed by the reduction of Cu_2O, not only in SAE but also in a conventionally used electrolyte (0.1 M KCl), though in 0.1 M KCl, the reductions of Cu_2O and CuO occurred

simultaneously, to a greater or lesser extent. As predicted, a $Cu/Cu_2O/Cu$ sandwich structure could be obtained by a partial reduction of the $CuO/Cu_2O/Cu$ sample.

Chapter 4 deals with further applications of the developed method to copper corrosion products other than oxides, which include sulfides, hydroxide, and "patina". Firstly, the voltammetric technique using SAE was applied to the simultaneous determination of oxides and sulfides of copper. It was found that the reduction peak of Cu_2S was well separated from those of oxides and appeared at a slightly higher potential than that of Cu_2O. Consequently, the three peaks of Cu_2O, Cu_2S, and CuO were sufficiently separated. It was also found that the reduction peak of Cu_9S_5 appeared at a potential slightly higher than that of Cu_2S.

Compared with these oxides and sulfides, $Cu(OH)_2$ and "patina" have less often been subjected to electrochemical detection by CP or LSV. In the voltammetry using SAE, however, well-defined peaks of $Cu(OH)_2$ and a basic copper sulfate $\{Cu_3(SO_4)(OH)_4\}$ could be obtained at slightly higher potentials than that of CuO. It should be noted that these species were difficult to reduce in 0.1 M KCl.

As shown in chapter 5, LSV with SAE has been successfully applied to clarify the mechanism for atmospheric corrosion of copper, in which $Cu(OH)_2$ played an initial key role. That is, $Cu(OH)_2$ was firstly formed on an uncorroded surface in the initial stage of atmospheric corrosion, and then converted to CuO in the corrosion process. Prolonging the corrosion period no longer enhanced the peak of CuO. Instead, the reduction peak of Cu_2O appeared and then grew with time. The CuO layer formed in the early stage of corrosion grew again after the growth of the Cu_2O layer stopped. Referring to the previous discussion, we have thus assumed that the limiting thickness of the Cu_2O layer results from the competition of the proportionation reaction ($Cu + CuO \rightarrow Cu_2O$) and the CuO formation ($Cu_2O + (1/2)O_2 \rightarrow 2CuO$).

In the final chapter, an application of the developed method to tin is described. In an ammonia buffer solution (0.5 M NH_4OH + 0.5 M NH_4Cl), well-defined reduction peaks for SnO and hydrated SnO_2 (denoted as $SnO_2 \cdot nH_2O$) were observed in the current-potential curve. The peak

potentials were fully separated by ~0.3 V, probably because NH_4^+ ions facilitated the reduction of $SnO_2 \cdot nH_2O$. In a borate buffer solution frequently used as a supporting electrolyte for this purpose, however, the peak of $SnO_2 \cdot nH_2O$ was not clearly detected. Using the ammonia buffer solution, we then found that the main corrosion products formed on tin in air were SnO and $SnO_2 \cdot nH_2O$. It was also found that SnO was formed in air at a temperature higher than 100 °C, while $SnO_2 \cdot nH_2O$ was formed at a temperature below 100 °C with a higher relative humidity 90%.

Acknowledgements

This doctoral thesis summarizes a series of studies on the characterization of corrosion copper products formed on copper. The studies have been conducted since 1998 in the Analysis Technology Research Center, Sumitomo Electric Industries (SEI), Ltd., Osaka, Japan. I wish to thank my colleagues in SEI, Ltd. (Mrs. Tokiko Umemoto, Dr. Atsushi Kimura, Mr. Junichi Matsumoto, and Mr. Takayasu Sugihara), and also thank Professor Susumu Kuwabata (Osaka University) and Mr. Masahiro Shibata (Tokai Rubber Industries, Ltd.), who partly contributed to this work. I also thank to Mr. Mitsuaki Nishie, the fellow at SEI, Ltd., for encouraging me to perform the studies, and Mr. Masayuki Nishimura, for warmly encouraging me to submit this doctoral thesis for assessment. The author is especially indebted to Dr. Takenori Notoya (technical advisor at Japan Copper and Brass Association) and Dr. Toshiyuki Osakai (Associate Professor at Kobe University) for valuable advice and discussions during the past decade.

List of publications

Publication Relevant to the present study

1. Shigeyoshi Nakayama, Atsushi Kimura, Masahiro Shibata, Susumu Kuwabata, and Toshiyuki Osakai, Voltammetric Characterization of Oxide Films Formed on Copper in Air, *J. Electrochem. Soc*., **148**, B467-B472 (2001).

2. Shigeyoshi Nakayama, Masahiro Shibata, Takenori Notoya, and Toshiyuki Osakai, On Standardizing to Voltammetric Determination of Cupric and Cuprous Oxides Formed on Copper, *Bunseki Kagaku*, **51**, 1145-1151 (2002).

3. Shigeyoshi Nakayama, Tokiko Kaji, Takenori Notoya, and Toshiyuki Osakai, Mechanistic Study of the Reduction of Copper Oxides in Alkaline Solutions by Electrochemical Impedance Spectroscopy, *Electrochim. Acta*, **53**, 3493-3499 (2008).

4. Shigeyoshi Nakayama, Tokiko Kaji, Masahiro Shibata, Takenori Notoya, and Toshiyuki Osakai, Which Is Easier to Reduce, Cu_2O or CuO?, *J. Electrochem. Soc*., **154**, C1-C6 (2007).

5. Shigeyoshi Nakayama, Tokiko Kaji, Takenori Notoya, and Toshiyuki Osakai, Quantitative Analysis of Copper Sulfides by Voltammetry Using a Strongly Alkaline Solution, *Zairyo-to-Kankyo*, **57**, 327-333 (2008), in Japanese; the English translation is available in *Corros. Eng.*, **57**, 419-431 (2008).

6. Shigeyoshi Nakayama, Masahiro Shibata, Susumu Kuwabata, Toshiyuki Osakai, and Takenori Notoya, Voltammetric Characterization of the Growth of Oxide Films Formed on Copper in Air, *Zairyo-to-Kankyo*, **51**, 566-570 (2002), in Japanese; the English translation is available in

Corros. Eng., **51**, 787-796 (2002).

7. Shigeyoshi Nakayama, Takenori Notoya, and Toshiyuki Osakai, A Mechanism for the Atmospheric Corrosion of Copper Determined by Voltammetry with a Strongly Alkaline Electrolyte, *J. Electrochem. Soc*., **157**, C289-C294 (2010).

8. Shigeyoshi Nakayama, Takayasu Sugihara, Junichi Matsumoto, Takenori Notoya and Toshiyuki Osakai, Chemical State Analysis of Tin Oxide Films by Voltammetric Reduction, *J. Electrochem. Soc*., **158**, C341 (2011).

Related papers

Shigeyoshi Nakayama, Masahiro Shibata, Toshiyuki Osakai, and Takenori Notoya, Voltammetric Chemical State Analysis of Copper Oxides and Hydroxide in Powder Samples, *Journal of the JRICu*, **43,** 235-239 (2004).

Shigeyoshi Nakayama, Takenori Notoya, and Toshiyuki Osakai, Instructions for Voltammetric Determination of Copper Corrosion Products Using a Strongly Alkaline Electrolyte, *Journal of the JRICu*, **49,** 273- 277 (2010).

Shigeyoshi Nakayama, Takenori Notoya, and Toshiyuki Osakai, Highly Selective Determination of Copper Corrosion Products by Voltammetric Reduction in a Strongly Alkaline Electrolyte, *Anal. Sci*., **28**, 323-331 (2012).

Takenori Notoya, Shigeyoshi Nakayama and Toshiyuki Osakai, "Benzotriazole–An Corrosion

Inhibitor for Copper and Its Alloys", 2008, Japan Association of Corrosion Control, Tokyo.

Shigeyoshi Nakayama, Mechanistic Study by Electrochemical Impedance Spectroscopy on Reduction of Copper Oxides in Neutral Solutions, *SEI Tech. Rev.*, **68**, 62-68 (2009).

S. Nakayama and T. Tokiko, Quantitative Analysis of Copper Sulfides by a New Electrochemical Method, *SEI Tech. Rev.*, **74**, 8-14 (2012).